Renewable and Sustainable Energy Reviews 16 (2012) 3154–3175

Contents lists available at SciVerse ScienceDirect

Renewable and Sustainable Energy Reviews

journal homepage: www.elsevier.com/locate/rser

A review of turbulence promoters used in solar thermal systems

Sunil Chamoli[a,*], N.S. Thakur[a], J.S. Saini[b]

[a] Centre For Excellence in Energy and Environment, National Institute of Technology, Hamirpur-177005, India
[b] Department of Mechanical and Industrial Engineering, Indian Institute of Technology, Roorkee-247667, India

ARTICLE INFO

Article history:
Received 24 November 2011
Received in revised form
18 December 2011
Accepted 5 January 2012
Available online 23 March 2012

Keywords:
Heat exchanger
Air heater
Solar energy
Ribs
Porous
Perforated baffles
Delta winglet

ABSTRACT

In order to enhance rate of heat transfer to flowing air in the duct of solar air heater and in heat exchanger or in cooling of turbine blade various turbulence generators viz. ribs, baffles and delta winglets are considered as an effective technique. Investigators reported various turbulence generators in literature for studying heat transfer, friction characteristics and flow pattern in heat exchanger and in solar air heater. In the present article an attempt has been made to categorize and review the reported turbulence generators used for heat transfer enhancement in heat exchanger and solar air heater and gives an approach for further research for forced convection from the surfaces with large scale roughness.

Contents

* Corresponding author. Tel.: +91 9816397033; fax: +91 1972 304728.
E-mail address: mech.chamoli@gmail.com (S. Chamoli).

1364-0321/$ – see front matter © 2012 Elsevier Ltd. All rights reserved.
doi:10.1016/j.rser.2012.01.021

1. Introduction

Heat transfer enhancement in a single phase at low and moderate Reynolds number has been a major subject of intensive research over the years. It has numerous applications including cooling of electronics systems, internal cooling inside turbine blades, compact heat exchangers, biomedical devices, solar air heater, etc. Many techniques based on both active and passive methods have been proposed to enhance heat transfer in these applications. Among these methods one can find systems involving vortex generators such as ribs and baffles. Disturbance promoters increase fluid mixing and interrupt the development of thermal boundary layer, leading too enhancement of heat transfer. Due to limited conventional energy resources an alternative finding is necessary, as energy in various forms has been playing an increasingly important role in world wide economic progress and industrialization. The growth of world population coupled with rising material needs has escalated the rate of energy usage. Rapid increase in energy usage characteristic of the past 50–100 years cannot continue indefinitely, as finite energy resources of earth are exhaustible. On the other hand, environment degradation with the use of fossil fuels is a threat to life on this planet earth. In view of world's depleting fossil fuel reserves and environmental threats, development of renewable energy sources has received an impetus. Of many alternatives, solar energy stands out as brightest long range resource for meeting continuously increasing demand for energy. It is considered to be a dominating renewable energy source due to its large potential. The freely available solar radiation provides an infinite and non-polluting reservoir of fuel. The simplest method to utilize solar energy for heating applications is to convert it into thermal energy by using solar collectors. Solar water heaters and solar air heaters are flat plate collectors which are generally used for heating water and air respectively. Solar air heaters are considered to be compact and less complicated as compared to solar water heaters. These are also free from corrosion and freezing problems. Solar air heater can be fabricated using cheaper as well as lesser amount of material and is simpler to use than solar water heater. Solar air heaters are generally considered to be useful for applications including space heating, crop drying, seasoning of timber, etc. A solar air heater occupies an important place among solar thermal systems because of minimal use of materials and cost. The thermal efficiency of a solar air heater is generally considered to be less because of low rate of heat transfer capability between absorber plate and air flowing in the duct. In order to make a solar air heater more effective solar energy utilization system, thermal efficiency needs to be improved by enhancing heat transfer rate. Advances in modern electronics have led dramatic increases in the level of heat fluxes that must be removed to ensure the reliable operation of electronics packages. Conventional cooling methods that are based on forced convection are as follows: (a) Placing ribs periodically on the heat transfer surface disturbs the boundary layer. These ribs are small and do not disturb the core flow so most of the turbulence enhancement and boundary layer breakdown are localized near the heat transfer surface. (b) Inserting baffles into the heat transfer devices promotes mixing of the coolant. These baffles can significantly disturb the bulk flow. Generally increased heat transfer coefficient is accompanied with increase in friction factor. Thus engineers and designers have been trying to optimize the geometry to yield a best heat transfer coefficient for either a given coolant or flow rate or an available pressure drop. In the present article an attempt has been made in order to make a brief outline of the performance enhancement of heat exchanger and solar air heater with turbulence promoters and vortex generators and gives an approach to modify the large scale roughness shapes and the usage of perforation for obtaining optimum design parameters at lowest pressure penalty.

2. Performance analysis

2.1. Conventional solar air heater

It is necessary to analyze the thermohydraulic performance of a solar air heater for making an efficient system. Thermal performance concerns with heat transfer process within the collector and hydraulic performance concerns with pressure drop in the duct. A conventional solar air heater shown in Fig. 1 is considered for brief analysis of thermal and hydraulic performance in the following sections. Design and construction detail of such type of a conventional system are described by Garg and Prakash [1].

2.1.1. Thermal performance of solar air heater

In order to evaluate thermal performance of a solar air heater, following Hottel–Whillier–Bliss equation reported by Duffie and Beckman [2] is commonly used.

$$Q_u = A_s F_R[I(\tau\alpha)_e - U_L(T_i - T_a)] \quad (1)$$

or

$$q_u = \frac{Q_u}{A_s} = F_R[I(\tau\alpha)_e - U_L(T_i - T_a)] \quad (2)$$

The rate of useful energy gain by the flowing air through duct of a solar air heater may also be calculated by using the following equation:

$$Q_u = \dot{m}C_p(T_o - T_i) = hA_s(T_{pm} - T_{fm}) \quad (3)$$

As discussed above, heat transfer coefficient (h) is represented in non-dimensional form by using relationship of Nusselt number (Nu) reported by Duffie and Beckman [2].

$$\mathrm{Nu} = \frac{hL}{k} \quad (4)$$

Furthermore thermal efficiency of a solar air heater can be expressed by the following equation:

$$\eta_{th} = \frac{q_u}{I} = F_R\left[(\tau\alpha)_e - U_L\left(\frac{T_i - T_a}{I}\right)\right] \quad (5)$$

The above equation shows that the plot between η_{th} and parameter $((T_i - T_a)/I)$ can be approximated by a straight line, of which intercept and slope are given by the values of $F_R(\tau\alpha)_e$ and $F_R U_L$ respectively.

2.1.2. Hydraulic performance

Hydraulic performance of a solar air heater concerns with pressure drop (ΔP) in the duct. Pressure drop accounts for energy consumption by fan to propel air through the duct. Pressure drop

Nomenclature

A_s	surface area of absorber plate, m^2
C_p	specific heat of air, J/kg K
D, D_h	equivalent or hydraulic diameter of duct, m
d, d'	print diameter of dimple/protrusion or geometric parameter of broken rib, m
e	rib height, m
g	groove position, m
h	heat transfer coefficient, W/m^2 K
H	depth of air duct, m
I	intensity of solar radiation, W/m^2
k	thermal conductivity of air, M/m K
L	length of test section of duct or long way length of mesh, m
m	mass flow rate, kg/s
p	pitch, m
ΔP	pressure drop, Pa
Q_u	useful heat gain, W
q_u	useful heat flux, W/m^2
S	length of discrete rib or short way length of mesh, m
T_o	fluid outlet temperature, K
T_i	fluid inlet temperature, K
T_a	ambient temperature, K
T_{pm}	mean plate temperature, K
T_{fm}	mean air temperature, K
U_L	overall heat loss coefficient, W/m^2 K
v	velocity of air in the duct, m/s
w	width of rib, m
W	width of duct, m

Dimensionless parameters

B/S	relative roughness length
B_h/D_h	window cut ratio
B_t/D_h	baffle thickness to hydraulic diameter ratio
d/w	relative gap position
d/D	relative print diameter
e^+	roughness Reynolds number
e/D, e/D_h	relative roughness height
e/H	rib to channel height ratio
f	friction factor
$\bar{f}$	average friction factor
F_R	heat removal factor
g/e	relative gap width
g/p	relative groove position
G	momentum heat transfer function
L/e	relative long way length of mesh
l/s	relative length of metal grit
Nu	Nusselt number
Nu_s	Nusselt number for smooth channel
Nu_r	Nusselt number for rough channel
Nu_{av}	area averaged Nusselt number
p/e	relative roughness pitch
P/H	baffle pitch spacing
PPI	pores per linear inch in each direction
Pr	Prandlt number
R	roughness function
Re	Reynolds number
St	Stanton number
$\overline{St}$	average Stanton number
S/e	relative short way length of mesh
W/H	duct aspect ratio

Greek symbols

Φ	rib chamfer/wedge angle, degree
η_{th}	thermal efficiency
η_{eff}	effective thermal efficiency
μ	dynamic viscosity, Ns/m^2
ρ	density of air, kg/m^3
α	angle of attack, degree
$(\tau\alpha)_e$	effective transmittance absorptance product
β	open area ratio

can be represented in non-dimensional form by using the following relationship of friction factor (f), reported by Frank and Mark [3].

$$f = \frac{(\Delta P)D_h}{2\rho L V^2} \tag{6}$$

2.1.3. Thermohydraulic performance

It is desirable that design of collector should be made in such a way that it should transfer maximum heat energy to the flowing fluid with minimum consumption of fan energy. Therefore in order to analyze overall performance of a solar air heater, thermo-hydraulic performance should be evaluated by considering thermal and hydraulic characteristics of the collector simultaneously.

3. Methodology of small height roughness elements

Surface roughness considered as most popular technique to enhance forced convection heat transfer. Initially, investigators speculated that elevated heat transfer coefficients might accompany the relatively high friction factors characteristic of rough conduits. However, since commercial roughness is not well defined, artificial surface roughness has been employed. Integral roughness may be produced by the traditional manufacturing processes of machining, forming, casting, or welding. Various inserts can also be used to provide surface protuberances in blade cooling passages, repeated roughness elements in the form of regularly spaced ribs are used to increase heat transfer rates. As a by-product of the desired increases in heat transfer rates, the pressure losses through the channel also increase. It is usually necessary to determine the best combination of heat transfer rate increases with the lowest possible pressure losses. The roughness is also used in heat exchanger and solar air heater to enhance rate of heat transfer. In solar air heater, the presence of laminar sublayer between absorber plate and flowing air is considered as a thermal resistance for heat transfer. Artificially roughened absorber plate in forms of ribs is

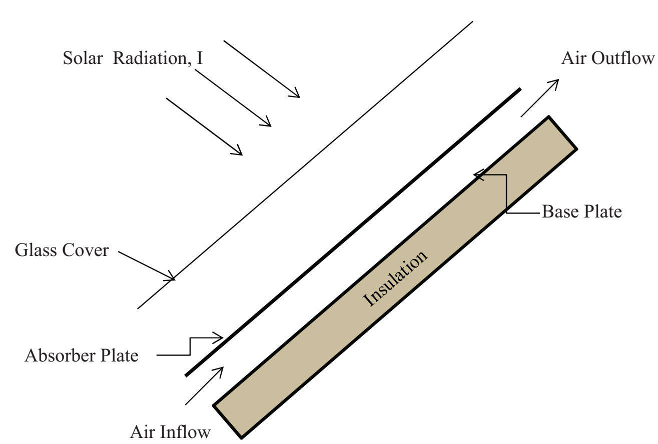


Fig. 1. Schematic diagram of conventional solar air heater.

considered as a viable methodology to break laminar sublayer in order to enhance rate of heat transfer. The ribs or wires break the laminar sublayer and create turbulence due to flow separation and reattachment between consecutive ribs, which reduce the thermal resistance and thus increase the rate of heat transfer. A considerable increase in friction losses also takes place thus the creation of turbulence is desirable only in the region very close to heat transferring surface i.e. up to laminar sublayer, for this purpose the small height is considered for ribs.

Attempt to increase heat transfer coefficient by small height roughness has been reported from over a century. Nikuradse in 1950 attempted to develop velocity and temperature distribution for roughened surfaces. Bergles et al. [4] reported significant improvement in heat transfer coefficient for in tube condensation of steam, when a wire was inserted in the cooling water jacket and spiraled around the condenser tube. There after many experimental investigations on roughness geometries have been carried out in the field of gas turbine airfoil cooling system, gas cooled nuclear reactors and design of compact heat exchangers. Different roughness geometries viz. regular and irregular shape are used in the investigations. A review of the roughness geometries used in solar air heater is reported by Varun et al. [29], Hans et al. [95] and Bhushan and Singh [107]. Application of artificial roughness methodology in a solar air heater for improvement of thermal performance owes its origin to these investigations.

4. Small height turbulence promoters used in heat exchangers

In regular roughness geometries different shapes, sizes and arrangements of roughness elements are studied in heat exchanger equipments. Mittal et al. [5] reported that early studies beginning with that of Nikuradse in 1950 attempted to develop velocity and temperature distribution for roughened surfaces. Special functions known as heat transfer function and momentum transfer function have been proposed to correlate data on heat transfer and fluid flow characteristics. Webb and Eckert [6] developed heat transfer and friction factor correlations for turbulent air flow in tubes having rectangular repeated rib roughness based on the law of wall similarity and application of the heat-momentum transfer analogy to flow over rough surface having relative roughness height of 0.01–0.04 at a relative roughness pitch of 10–40 and range of Prandtl number of 0.71–37.6. Lewis [7] defined new efficiency parameter for optimizing thermohydraulic performance of rough surfaces. General arrangement of different types of roughness geometries reported by various investigators can be divided into four categories i.e. (a) transverse/inclined or discrete ribs, (b) continuous/discrete V shaped rib, (c) dimple/protrusion formation and (d) rib cross-section.

4.1. Transverse/inclined or discrete ribs

Small height wires as roughness element are frequently used in heat exchanger for heat transfer enhancement. Hu and Shen [19] investigated the effect of inclined discrete ribs with and without groove and reported performance improvement for discrete arrangement without groove. Cho et al. [20] examined the effect of angle of attack and number of discrete ribs in rectangular duct and reported that gap region between discrete ribs accelerates the flow and results an increase in local heat transfer coefficient. Hong and Hsieh [30] carried out experimental study on heat transfer and friction factor characteristics of developing and fully developed turbulent air flow in a square duct with two opposite rib roughened walls which are attached in a staggered manner. It was found that the heat transfer rate is 2.02–4.60 times as high as that of fully developed smooth duct flow for the lowest Reynolds number of the study i.e. 13,000. Park et al. [31] investigated the combined effects of the channel aspects ratio, rib angle of attack, and flow Reynolds number on heat transfer and pressure drop in rectangular channels with two opposite ribbed walls. The study reveals that the narrow aspect ratio $W/H < 1$ gives much better heat transfer performance than the wide aspect ratio $W/H > 1$. Murata and Mochizuki [33] carried out numerical simulation of heat transfer in rib roughened rectangular duct by using second order finite difference method in coordinates fitted to transverse or angled ribs. It was found that the turbulent cases of both 60° and 90° ribs, the flow reattachment at the midpoint between the ribs and the unsteady reverse flow in front of the rib formed high values of the time averaged heat transfer, especially the heat transfer in front of the rib became very high. Tariq et al. [34] carried out experimental study to investigate the heat transfer and flow characteristics in the entrance region of a rectangular channel with a single and two solid square ribs mounted on the bottom surface of the channel and found that the maximum value of Urms is observed to increase in the stream-wise direction and then decrease subsequently for the one-rib case. For the two-rib case, the Urms is observed to increase second time after the second rib. But, the increase in magnitude is less significant than that after the first rib. Tatsumi et al. [35] carried out numerical simulation for flow and thermal fields over two types of arrays viz. full span and discrete ribs attached to a channel wall and found that the discrete rib case, flows going by the rib accompany a pair of counter-rotating large scale stream-wise vortices and enhances the flow mixing that keeps the wall heat transfer higher. Tornado type transverse vortices appearing behind the edge of the rib become more intense and larger in scale in the duct roughened with discrete ribs. Generation of this type of vortices is effective to reduce the area of the flow recirculation region and is effective to enhance the wall heat transfer. An optical technique to measure local heat transfer coefficients in continuous and discrete transverse ribs as shown in Fig. 2 was studied by Cavallero and Tanda [36]. The technique is based on the use of thermo chromic liquid crystals applied to the test surface. It was found that the surface ribbed by continuous ribs with the lower pitch-to-height ratio ($p/e = 4$) showed a progressively increasing heat transfer coefficient, along the stream-wise coordinate, in the inter-rib region and for the higher pitch-to-height ratio ($p/e = 8$), the local heat transfer coefficient reached a relative maximum, probably at the reattachment point, followed by a slight reduction in the stream-wise direction and by a further increase close to the successive rib.

Wong et al. [37] conducted experimental and numerical studies to investigate the forced convection and flow friction of a turbulent airflow in a horizontal air-cooled rectangular duct, with square-sectioned cross-ribs mounted on its bottom surface with angle 30° and 120°. It was found that experimental and numerical studies, use of cross-ribs could be a promising solution to enhance the forced convection in a rectangular duct. The ability of the cross-ribbed surface to enhance forced convection was found to be better than the well-known parallel-ribbed surface. Won and Ligrani [39] investigate spatially resolved-local flow structure, spatially averaged flow structure, and surface Nusselt numbers are presented and compared for stationary channels with aspect ratios of 4 and rib turbulators inclined at 45° for two different rib arrangements with perpendicular and parallel orientations on two opposite surfaces are considered for investigation. It was found that Local Nusselt number ratios are roughly the same for the crossed and parallel rib configurations for all locations along the test surface, except just upstream of the ribs; here local parallel rib Nusselt number ratio is significantly higher than local crossed rib ratios; this is due to significantly different overall and local secondary flows for the two rib configurations, especially secondary flows events with length

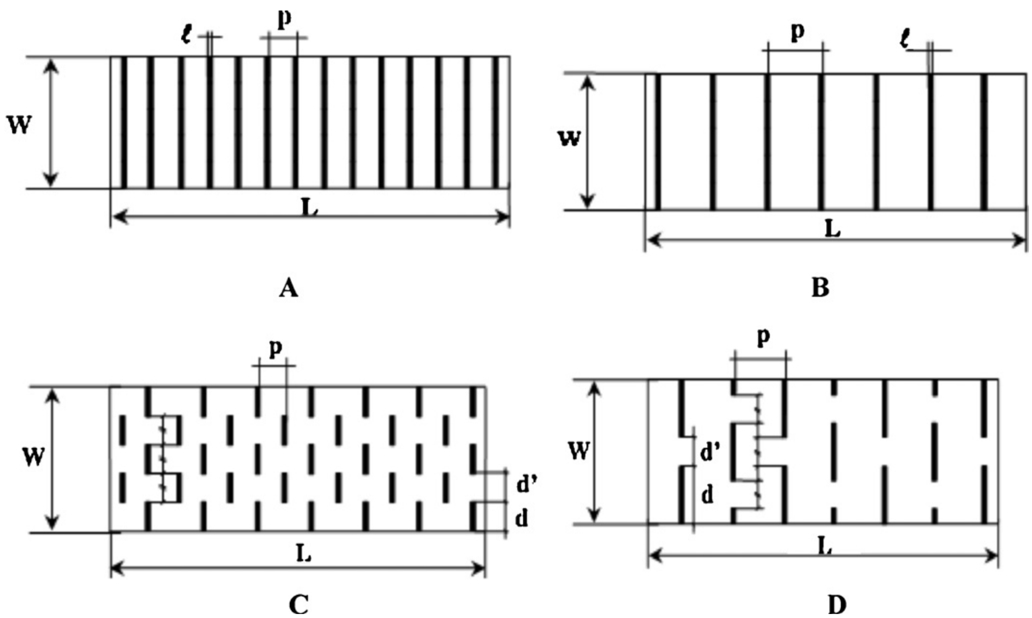


Fig. 2. Top view of rib configuration studied.

scales which are of the order of the span-wise spacing between adjacent ribs. Lu and Jiang [40] carried out a numerical and experimental investigation of forced convection heat transfer of air in a rectangular channel with 45° inclined ribs. It was observed that geometry with ribs 4 mm apart on one wall, the channel with 60° ribs had the best heat transfer performance, the channel with 0° ribs had the least pressure drop, and the channel with 20° ribs had the best thermo hydraulic performance. Tanda [45] carried out experimental investigation of forced convection in a rectangular channel of AR = 5 with angled rib turbulators inclined at 45° by using liquid crystal thermography. It was found that for the one-ribbed wall channel, the degree of enhancement of the friction factor, relative to the smooth channel, is between 2.6 and 4.3; when ribs are present on two opposite walls, the friction factor ratio f/f_0 is greatly enhanced (from 6.9 to 14.3), becoming about three times higher as compared with the one-ribbed wall channel. Values of f/f_0 tend to slightly increase with increasing Reynolds number and to decrease with increasing rib pitch-to-height ratio and the rib pitch-to-height ratio $p/e = 13.33$ is still the optimum value for the one-ribbed wall channel (with heat transfer augmentation, for the investigated range of Reynolds number, between 1.25 and 1.45), while the largest gain in performance is provided by $p/e = 10$ for the two-ribbed wall channel (heat transfer augmentation in the 1.02–1.20 range).

4.2. Continuous/discrete V shaped rib roughness

The inclined rib gives better heat transfer than transverse one due to the secondary flow thus the investigators look towards the V shaped rib roughness. Han et al. [13] investigated the effect of parallel and V-shaped broken rib orientations on the local heat transfer distribution and pressure drop in a square channel with two opposite ribbed walls and found that 60° staggered discrete V-shaped ribs provide higher heat transfer than parallel discrete ribs. Lau et al. [15], Taslim et al. [16] and Olsson and Sunden [17] investigated the effect of V-shaped ribs in square channel and found enhancement in heat transfer as compared to inclined ribs and transverse ribs. Results showed that an average Stanton number for the inclined 45° and 60° discrete ribs was 20–35% higher than in 90° full rib case. Gao and Sunden [18] also reported that V-shaped ribs pointing downward perform better than the ribs pointing upward in rectangular ducts. Olsson and Sunden [32] carried out experimental investigation of secondary flow patterns, pressure drop and heat transfer in rib roughened rectangular channel of the geometries cross ribs, parallel ribs, cross V-ribs, and multiple v ribs and the flow patterns investigated with smoke wire visualization and LDV measurements as shown in Fig. 3. It was found that swirl flow tube provides a significant increase in the j and f factors for Reynolds numbers from 1000 and 2000, while at higher Reynolds numbers these are at the same level as those the most of the other rib-roughened channels. The high heat transfer enhancement in the low Reynolds number range is caused by a stable secondary flow. At Reynolds numbers above 4000, the highest j/f ratio of all channels tested is provided with the V-ribs pointing upstream, while the lowest j/f ratio is provided with the V-ribs pointing downstream Table 1.

Gao and Sunden [18] investigate the thermal and hydraulic performances of three rib-roughened rectangular ducts with three rib configurations parallel ribs and V shaped ribs pointing upstream or downstream of the main flow direction. Study reveals that V ribs pointing downstream produced the highest heat transfer enhancement and friction factors, and provided the best thermal performance over the tested Reynolds number range. Parallel ribs provided better performance than V ribs pointing upstream at high Reynolds number. Tanda [38] made investigations using liquid crystal thermography to obtain detailed distributions of heat transfer coefficient in rib-roughened channels. The roughness geometries induced by transverse continuous, transverse broken and V-shaped broken ribs were deployed on a heated surface as shown in Fig. 4. The highest value of enhanced Nusselt number was reported for the transverse broken ribs having relative roughness pitch (P/e) value of 4. Large increase in friction factor was induced by ribs as compared to the smooth channel.

Lee at al. [44] investigated effect of aspect ratio on heat/mass transfer in rectangular channels with two different V shaped rib configuration with a 60° attack angle and multiple (staggered) V shaped rib configuration with a 45° attack angle using naphthalene sublimation method. It was observed that 60° continuous V-shaped rib configurations, the heat/mass transfer coefficients showed the maximum values at the center region, and decreased gradually along the angled ribs due to the two pairs of large-scale counter-rotating secondary flows generated in the channel.

Table 1
Heat transfer coefficient and friction factor correlations for different turbulence promoters used in solar thermal systems.

Geometry	Authors	Range of parameters	Correlations	
			Heat transfer coefficient	Friction factor
A. Ribs Transverse Small diameter staggered arrangement	Hong and Hsieh [30]	e/D_h: 0.19 p/e: 5.31	$Nu = 0.056 Re_H^{0.74}$ (For Tu = 0.04) $Nu = 0.030 Re_H^{0.79}$ (For Tu = 0.07) $Nu = 0.019 Re_H^{0.83}$ (For Tu = 0.11)	
Small diameter protrusion wires	Prasad and Saini [47]	e/D: 0.020–.033 p/e: 10–20 Re: 5000–50,000	$\overline{S_t} = \bar{f}/2/1 + \sqrt{f/2}\{4.5(e^+)^{0.28} Pr^{0.57} - 0.95(p/e)^{0.53}\}$	$f_r = 2/[0.95(p/e)^{0.53} + 2.5\ \ln(D/2e) - 3.75]^2$
Small diameter transverse	Gupta et al. [52]	e/D: 0.018–.052 Re: 3000–18,000	$Nu = 0.000824(e/D)^{-0.178}(W/H)^{0.284} Re^{1.062} e \le 35$ $Nu = 0.00307(e/D)^{-0.469}(W/H)^{0.245} Re^{0.812} e \ge 35$	$f = 0.06412(e/D)^{0.019}(W/H)^{0.237} Re^{-0.185}$
Small diameter transverse protrusion wire	Verma and Prasad [50]	e/D: 0.01–0.03 p/e: 10–40 e^+: 8–42 Re: 5000–20,000	$Nu = 0.08596(p/e)^{-0.054}(e/D)^{0.072} Re^{0.723} e \le 24$ $Nu = 0.0245(p/e)^{-0.016}(e/D)^{0.021} Re^{0.802} e \ge 24$	$f = 0.0245(p/e)^{-0.0206}(e/D)^{0.021} Re^{-1.25}$
2. V shaped/inclined Wire ribs Inclined wire ribs	Gupta et al. [108]	e/D: 0.02–0.053 p/e: 7.5–10 α: 30–90° Re: 5000–30,000	$Nu = 0.000824(e/D)^{-0.178}(W/H)^{0.284} Re^{1.062}\ \exp[-0.04(1-\alpha/60)^2](k/D)e \le 35$ $Nu = 0.00307(e/D)^{-0.469}(W/H)^{0.245} Re^{0.812}\ \exp[-0.475(1-\alpha/60)^2](k/D)e \ge 35$	$f = 0.06412(e/D)^{0.019}(W/H)^{0.0237} Re^{-0.185}\ \exp[-0.0993(1-\alpha/60)^2]$
V shaped staggered Discrete wire ribs	Mulluwork et al. [53,54]	e/D: 0.02 α: 60° B/S: 3–9 Re: 2000–15,500	$Nu = 0.00534(B/S)^{1.3496} Re^{1.2991}$	$f = 0.7117(B/S)^{0.0636} Re^{-2.991}$
V shaped continuous Wire ribs	Momin et al. [55]	e/D: 0.02–0.034 p/e: 10 α: 30–90° Re: 2500–18,000	$Nu = 0.067(e/D)^{0.424}(\alpha/60)^{-0.077} Re^{0.888}\ \exp[-00782 \ln(\alpha/60)^2]$	$f = 6.266(e/D)^{0.565}(\alpha/60)^{-0.093} Re^{-0.425}\ \exp[-0.719 \ln(\alpha/60)^2]$
Inclined discrete and continuous wire ribs	Karwa [56]	e/D_h: 0.0467–0.05 p/e: 10 α: 60–90° B/S: 3 W/H: 7.19–7.75	$G = 32.26 e^{-0.006}(W/H)^{0.5}(p/e)^{2.56}\ \exp[0.7343 \ln(p/e)^2](e^+)^{0.08}$	For $7 \le e^+ \le 20 R = 1.66 e^{-0.0078}(W/H)^{-0.4}(p/e)^{2.695}\ \exp[-0.762\ \ln(p/e)^2 (e^+)^{-0.075}]$ For $20 \le e^+ \le 60 R = 1.325 e^{-0.0078}(W/H)^{-0.4}(p/e)^{2.695}\ \exp[-0.762\ \ln(p/e)^2 (e^+)^{-0.075}]$
Grid shaped wire Ribs	Karmare and Tikekar [57]	e/D_h: 0.035–.044 p/e: 12.5–36 l/s: 1.72–1 Re: 4000–17,000	$Nu = 2.4(e/D_h)^{0.42}(l/s)^{-0.146} Re^{1/3}(p/e)^{-0.27}$	$f = 15.55(e/D_h)^{0.94}(l/s)^{-0.27} Re^{-0.26}(p/e)^{-0.51}$
Inclined discrete ribs	Aharwal et al. [58]	p/e: 10 e/D_h: 0.0377 W/H: 5.87 Re: 3000–18,000 d/w: 0.167–0.5 α: 60°	$Nu = 0.0102(e/D)^{0.51} Re^{1.148}[\{1-(0.25-d/w)^2\{0.01(1-g/e)^2\}\}]$	$f = 0.5(e/D)^{0.72} Re^{-0.0836}$
Inclined and transverse wire ribs	Varun et al. [59]	Re: 2000–14,000 p/e: 3–8	$Nu = 0.0006(p/e)^{0.0104} Re^{1.213}$	$f = 1.0858(p/e)^{0.0114} Re^{-0.3685}$
Arc shaped wire ribs	Saini and Saini [60]	g/e: 0.5–2 p/e: 10 e/D: 0.0213–.0422 $\alpha/90$: 0.333–0.666 Re: 2000–17,000	$Nu = 0.001047(e/D)^{0.3772}(\alpha/90)^{-0.1198} Re^{1.3186}$	$f = 0.14408(e/D)^{0.1765}(\alpha/90)^{0.1185} Re^{-0.17103}$
Multiple V shaped	Hans et al. [61]	P/e: 6–12 e/D: 0.019–0.043 α: 30–75° Re: 2000–20,000 W/w: 1–10	$Nu = 3.35 \times 10^{-5} Re^{0.92}(e/D)^{0.77}(W/w)^{0.43}(\alpha/90)^{-0.49}\ \exp[-0.1177(Ln(W/w))^2]\ \exp[-0.61(Ln(\alpha/90))^2](P/e)^{8.54}\ \exp[-2.0407(Ln(P/e))^2]$	$f = 4.47 \times 10^{-4} Re^{-0.3188}(e/D)^{0.73}(W/w)^{0.22}(\alpha/90)^{-0.39}\ \exp[-0.52(\ln(\alpha/90))^2](P/e)^{8.9}\ \exp[-2.133(\ln(P/e))^2]$

Discrete V shaped	Singh et al. [62]	Re: 3000–15,000 P/e: 4–12 α: 30–75° d/w: 0.2–0.8 g/e: 0.5–2.0 e/D_h: 0.015–0.043	$\mathrm{Nu} = 2.36 \times 10^{-3} Re^{0.90} (P/e)^{3.50} (\alpha/60)^{-0.023} (d/w)^{-0.043} (g/e)^{-0.014} (e/D_h)^{0.47} \exp(-0.84(\ln(p/e))^2) \exp(-0.72(\ln(\alpha/60))^2) \exp(-0.05(\ln(d/w))^2) \exp(-0.15(\ln(g/e))^2)$	$f = 44.13 \times 10^{-2} Re^{-0.126} (P/e)^{2.74} (\alpha/60)^{-0.034} (d/w)^{-0.058} (g/e)^{-0.031} (e/D_h)^{0.70} \exp(-0.685(\ln(p/e))^2) \exp(-0.93(\ln(\alpha/60))^2) \exp(-0.058(\ln(d/w))^2) \exp(-0.21(\ln(g/e))^2)$
B. Wire mesh Expanded metal mesh	Saini and Saini [67]	l/e: 25–71.87 s/e: 15.62–46.87 e/D: 0.012–0.0390 Re: 1900–13,000	$\mathrm{Nu} = 4.0 \times 10^{-4} Re^{1.22} (e/D)^{0.625} (s/10e)^{2.22} \exp[1.25\{\ln(s/10e)\}^2] (l/10e)^{2.66} \exp[0.824\{\ln(l/10e)\}^2]$	$f = 0.815 Re^{0.361} (l/e)^{0.266} (s/10e)^{0.19} (10e/d)^{0.591}$
C. Machined Ribs Chamfered ribs	Karwa et al. [63]	e/D: 0.014–0.0320 p/e: 4.5–8.5 Re: 3000–20,000 Φ: −15, 0, 10, 15, 18 W/H: 4.8, 6.1, 7.8, 9.66, 12	$G = 103.77 e^{-0.006} (W/H)^{0.5} (p/e)^{2.56} \exp[0.7343\{\ln(p/e)\}^2] (e^+)^{-0.31}$ For $7 \le e^+ < 20$ $G = 32.26 e^{-0.006} (W/H)^{0.5} (p/e)^{2.56} \exp[0.7343\{\ln(p/e)\}^2] (e^+)^{0.8}$ For $20 \le e^+ \le 60$	For $7 \le e^+ \le 20$ $R = 1.66 e^{-0.0078} (W/H)^{-0.4} (p/e)^{2.695} \exp[-0.762\{\ln(p/e)\}^2 (e^+)^{-0.075}]$ For $20 \le e^+ \le 60$ $R = 1.325 e^{-0.0078} (W/H)^{-0.4} (p/e)^{2.695} \exp[-0.762\{\ln(p/e)\}^2]$
Wedge shaped ribs	Bhagoria et al. [64]	e/D: 0.015–0.033 Re: 3000–18,000 p/e: $60.17\phi^{-1.0264} < p/e < 12.12$ ϕ: 8–15°	$\mathrm{Nu} = 1.89 \times 10^{-4} Re^{1.21} (e/D)^{0.426} (p/e)^{2.94} \exp[-0.71\{\ln(p/e)\}^2] (\phi/10)^{-0.018} [\exp(-1.50(\ln(\phi/10)))^2]$	$f = 12.44 Re^{-0.18} (e/D)^{0.99} (p/e)^{-0.52} (\phi/10)^{0.49}$
Chamfered rib groove combination	Layek et al. [66]	Re: 3000–21,000 e/D: 0.022–0.04 p/e: 4.5–10 g/p: 0.3–0.6 ϕ: 5–30°	$\mathrm{Nu} = 0.002062 Re^{0.936} (e/D)^{0.349} (p/e)^{3.318} \exp[-0.868\{\ln(p/e)\}^2] (g/p)^{1.108} \exp[2.486\{\ln(g/p)\}^2 + 1.406\{\ln(g/p)\}^3]$	$f = 0.001227 Re^{-0.199} (e/D)^{0.585} (p/e)^{7.19} \exp[-1.854\{\ln(p/e)\}^2] (g/p)^{0.645} \exp[1.513\{\ln(g/p)\}^2 + 0.8662\{\ln(g/p)\}^3]$
D: Protrusions Dimple protrusions	Saini and Verma [68]	e/D: 0.018–0.037 p/e: 8–12 Re: 2000–12,000	$\mathrm{Nu} = 5.2 \times 10^{-4} Re^{1.27} (e/D)^{0.33} (p/e)^{3.15} \exp[-2.21\{\log(p/e)\}^2] \exp[-1.30\{\log(e/D)\}^2]$	$f = 0.0642 Re^{-0.423} (e/D)^{-0.0214} (p/e)^{-0.465} \exp[0.054\{\log(p/e)\}^2] \exp[-0.840\{\log(e/D)\}^2]$
Dimple-shape roughness	Bhushan and Singh [69]	S/e: 18.75–37.50 L/e: 25–37.5 d/D: 0.147–0.367 e/D: 0.03 Re: 4000–20,000	$\mathrm{Nu} = 2.1 \times 10^{-88} Re^{1.452} (S/e)^{12.94} (L/e)^{99.2} (d/D)^{-3.9} \exp[-10.4(\log(S/e))^2] \exp[-77.2(\log(L/e))^2] \exp[-7.83(\log(d/D))^2]$	$f = 2.32 Re^{-0.201} (S/e)^{-0.383} (L/e)^{-0.484} (d/D)^{0.133}$

			Heat transfer coefficient			Friction factor					
			$\mathrm{Nu}^+ = C_o + C_1 \times \mathrm{Re} \times 10^{-6}$			$B_t/D_h = 1/12$			$B_t/D_h = 1/12$		
						10PPI	20PPI	40PPI	10PPI	20PPI	40PPI
E: Porous bafflesPorous baffle	Ko and Anand [82]	B_h/D_h: 1/3, 2/3PPI: 10, 20, 40B_t/D_h: 1/12, 1/3	$B_h/D_h = 1/3$	NU^+	C_o	1.56	1.78	1.94	2.77	2.75	3.30
					C_1	−1.81	−6.95	−7.80	−17.13	−12.62	−20.93
			$B_h/D_h = 1/3$	NU^+	C_o	0.65	0.70	0.66	0.84	0.93	0.93
					C_1	−1.48	−3.08	−2.92	−6.19	−3.24	−6.89
			$B_h/D_h = 2/3$	NU^+	C_o	1.90	1.98	1.95	2.96	3.13	3.94
					C_1	−6.39	−8.78	−6.83	−13.17	−16.25	−38.55
			$B_h/D_h = 2/3$	NU^+	C_o	0.57	0.51	0.47	0.59	0.57	0.69
					C_1	−2.06	−2.16	−1.99	−3.63	−3.73	−7.21

F: Solid baffles Inverted U-shaped	Bopche and Tandale [76]	Re: 3800–18,000 e/D_h: 0.0186–0.03986 p/e: 6.67–57.14 α: 90°	$\mathrm{Nu} = 0.5429 \times Re^{0.7054} (e/D)^{0.3619} (p/e)^{-0.1592}$	$f = 1.2134 \times Re^{-0.2076} (e/D)^{0.3285} (p/e)^{-0.4259}$
Multiple 60° V shaped	Promvonge [77]	e/H: 0.10, 0.20, 0.30 P/H: 1, 2, 3 Re: 5000–25,000	$\mathrm{Nu} = 0.147 \times Re^{0.763} (\mathrm{PR})^{0.4} (1 - e/H)^{-1.793} (1 + \mathrm{PR})^{-0.42}$	$f = 0.48 Re^{-0.038} (1 - e/H)^{-5.428} (1 + \mathrm{PR})^{-0.833}$
G: Perforated Baffles Transverse perforated baffle	Karwa and Maheshwari [94]	Re: 2700–11,150 p/e: 7.21, 14.42, 28.84 β: 26%, 46.8% δ/e: 0.047	$\mathrm{Nu} = 0.0893 Re^{0.7608}$	$f = 0.1673 Re^{-0.0213}$

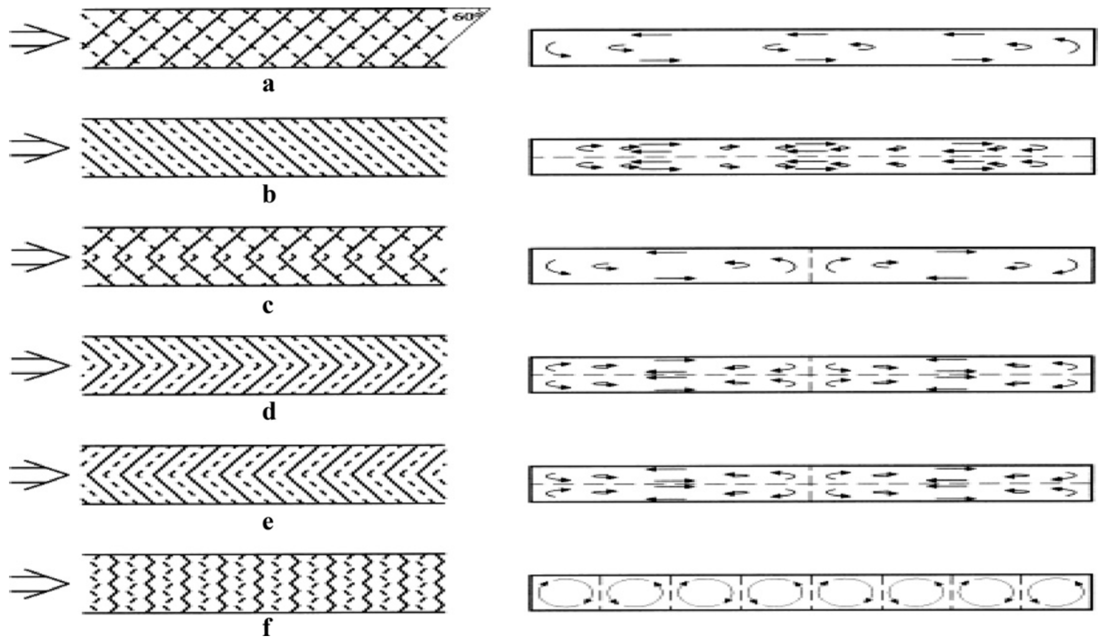


Fig. 3. Rib configurations and conjectured secondary flow patterns: (a) cross rib roughened, (b) parallel rib roughened, (c) cross v rib roughened, (d) parallel v rib roughened » (e) parallel v rib roughened « (f) swirl flow tube.

4.3. Dimple/protrusion formation

Generation of dimples/protrusions on surface of absorber plate is also considered to be a simple and economical methodology to create artificial roughness. It is a subject of many recent experimental investigations. Use of dimple shape roughness produced augmented surface heat transfer levels as compared to channels with smooth surfaces and at par with other artificial roughness geometries. On the other hand pressure drop or friction loss usually does not increase appreciably as compared to other rough channels.

Moon et al. [23] investigated effects of channel height on heat transfer in a rectangular duct with a dimpled surface and observed enhancement in heat transfer by about 2.1 times regardless of channel height and friction factor of 1.6–2.0 times that of smooth channel. Mahmood and Ligrani [24,25] measured local heat transfer on dimpled surface of opposite walls with various temperature ratios having ratio of channel height to dimple print diameter of 0.5 and observed that vortex structures augment local Nusselt number near downstream rim of each dimple. Burgess et al. [26] conducted an experimental study to investigate effect of dimple depth on heat transfer with aspect ratio of 8 and for Reynolds number range of 12,000–70,000 and reported that Nusselt number increases with increase in dimple depth. Sang et al. [27] investigated heat transfer with dimple/protrusion arrays in a rectangular duct with low Reynolds number range and observed heat transfer enhancement of 14 and 7 times for double protrusion wall and double dimpled wall at Reynolds number of 1000. However at high Reynolds number of 10,000, enhancement level observed was from 2 to 3. Chang et al. [28] examined heat transfer characteristics for four sets of dimpled channels with Reynolds number ranging from 1500 to 11,000 and determined effect of dimpled arrangement, fin

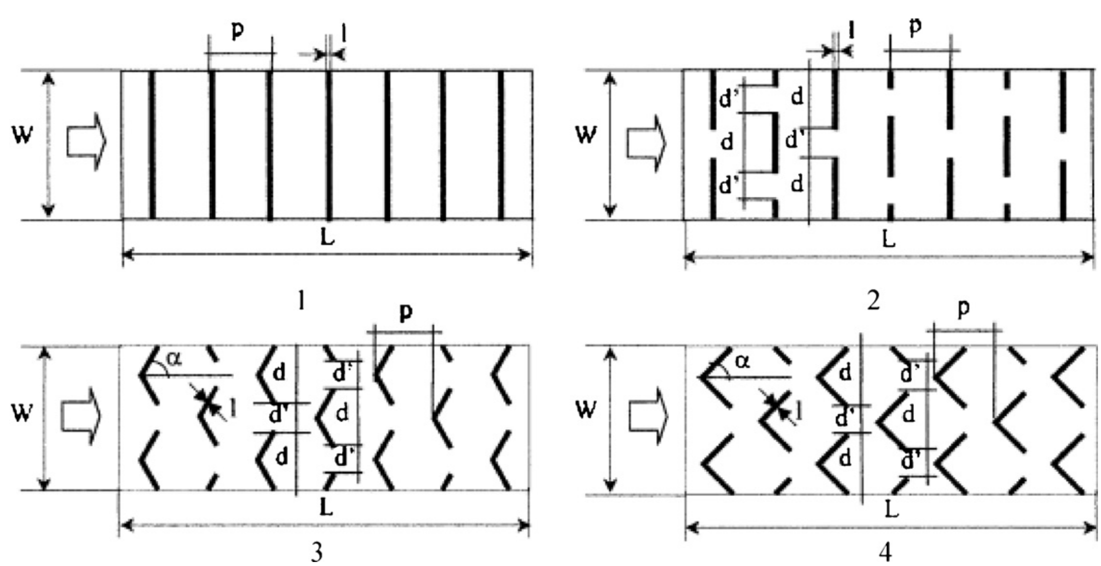


Fig. 4. Geometry of rib configuration studied – 1. Transverse continuous; 2. Transverse broken ribs; 3. Broken 60° v ribs; 4. Broken 45° v ribs.

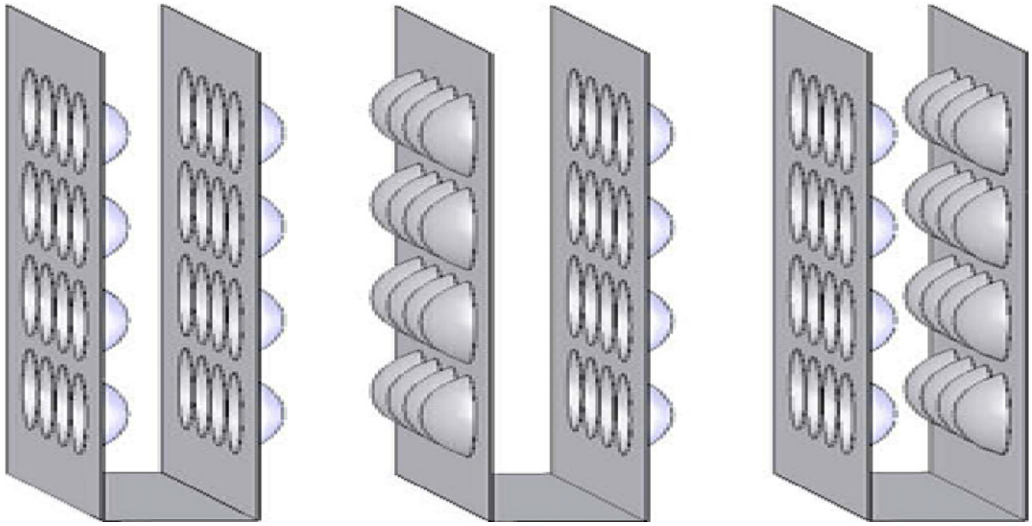


Fig. 5. (a) Concave convex channel; (b) concave concave channel; (c) convex convex channel.

length to channel hydraulic diameter ratio and Reynolds number on heat transfer over the dimpled fin channel as shown in Fig. 5.

4.4. Rib cross-section

The rib cross-section shapes such as square, rectangle, triangular, and semicircular were reported by the investigators Ravigururajan and Bergles [8] who developed general statistical correlations for heat transfer and pressure drop for four types of roughness elements such as semicircular, circular, rectangular and triangular for single-phase turbulent flow in internally ribbed tubes. Han [9–12] carried out an experimental study of the effect of rib shape, angle of attack, pitch to height ratio and spacing in square duct with two opposite rib roughened wall. Parallel full ribs having an angle of attack, 'α' of 45° and 30° had the best thermal performance. Liou and Hwang [14] reported experimental study on turbulent heat transfer and friction in a channel having ribs of semicircular, square and triangular shapes and mounted on two opposite walls. For the range of Reynolds number studied, ribs of semicircular, triangular and square shape yielded about 1.6–2.0, 1.7–2.2 and 1.9–2.7 fold increase in average Nusselt number while friction factor increased by 4–8, 5–10 and 7–15 fold respectively. Chyu et al. [21,22] reported local heat transfer measurements on ribs of hemispherical and teardrop shapes by using a transit liquid crystal technique and obtained 2.5 times greater heat transfer enhancement, and air pressure penalty is half the values produced by conventional rib turbulator. Kamali and Binesh [41] conducted numerical investigation of the turbulent heat transfer and friction factor in a square duct with various shaped ribs mounted on one wall with four different ribs configuration viz. square, triangular, trapezoidal with decreasing height in flow direction, trapezoidal with increasing height in flow direction. It was observed that for the range of Reynolds number the trapezoidal rib with decreasing height in the flow direction has the highest value of heat transfer, while the case D has the lowest value of friction factor and $p/e = 12$ provides the highest enhancement factor among the four pitch investigated. Promvonge and Thianpong [42] carried out experimental investigation of turbulent forced convection heat transfer and friction loss behaviors for air flow through a constant heat flux channel fitted with different shaped ribs shown in Fig. 6. The ribs cross sections used in this study are triangular (isosceles), wedge (right triangular) and rectangular shapes and both inline and staggered arrangements were used. It was observed that rib turbulators with $e/H = 0.3$ cause a very high pressure drop increase, especially for inline rib arrangement and also provide considerable heat transfer augmentation, $Nu_a/Nu_o = 2.6–4.4$, depending on rib geometry and Nusselt number augmentation tends to increase with the rise of Reynolds number. The staggered triangular rib should be applied instead of the rectangular one to obtain higher heat transfer and performance of about 50–65% leading to more compact heat exchanger. The best operating regime for all rib turbulators is found at the lowest Reynolds number values.

Thianpong et al. [43] carried out experimental investigation of turbulent heat transfer and friction loss behaviors of airflow through a constant heat-fluxed channel fitted with different heights of triangular ribs and the rib cross section geometry used in the present study was isosceles triangle. It was observed that use of rib turbulators causes a very high pressure drop increase, especially for high flow blockage rib, $e/H = 0.26$ and also provides considerable heat transfer augmentations, $Nu/Nu_o = 1.8–4.0$, depending on rib height.

5. Roughness geometries used in solar air heater

In solar air heaters, artificial roughness in the form of attaching the small diameter wires, machining ribs of different shapes, forming dimples/protrusion have been investigated for performance enhancement of solar air heater. There are many parameters that characterize the arrangement and shape of the roughness elements; height (e) and pitch (P) of roughness element are the most

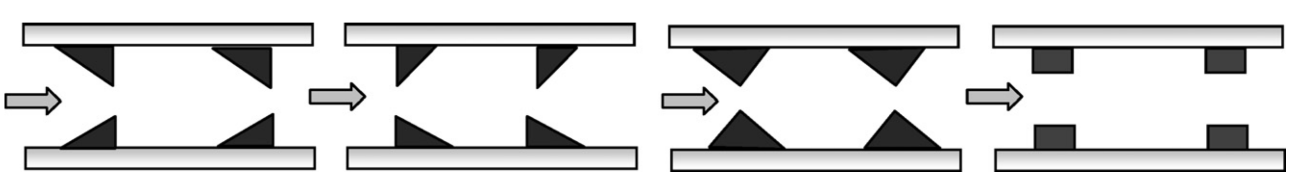


Fig. 6. Test section with inline rib arrangements (a) wedge pointing upstream; (b) wedge pointing downstream; (c) triangular; (d) rectangular.

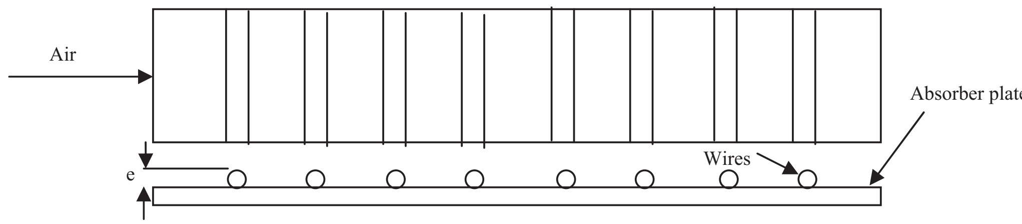


Fig. 7. Roughened absorber plate with transverse continuous ribs.

important parameters. These are specified in non-dimensional form as relative roughness height (e/D) and relative roughness pitch (P/e) respectively. The other parameters include Reynolds number, rib cross-section, angle of attack, chamfering and combined turbulence promoters. Literature on application of artificial roughness in a solar air heater covers wide range of roughness geometries for studying heat transfer and friction characteristics. General arrangement of different types of roughness geometries reported by various investigators can be divided into four categories i.e. (i) wire fixation, (ii) rib formation by machining process, (iii) wire mesh or expanded metal mesh fixation and (iv) dimple/protrusion formation. These have been discussed in detail under the following sections.

5.1. Wire fixation

Various investigators studied heat transfer enhancement and friction factor by fixing protruding wires of different shape, size and orientation as an artificial roughness element on absorber plate as has been discussed below.

5.1.1. Transverse continuous ribs

Kays [46] proposed fixing small diameter protrusion wires perpendicular to flow direction on surface of absorber plate break laminar sub-layer. It was suggested that protrusion wire diameter of $y^+ = 50$, spaced 10–20 times diameter and placed within the laminar sub-layer are better than turbulence promoters. Prasad and Saini [47,48] develop empirical correlations for heat transfer coefficient and friction factor for fully developed turbulent flow in a solar air heater duct having absorber plate roughened artificially by small diameter wires as shown in Fig. 7 of various relative roughness heights ranging from 0.020 to 0.033 and relative roughness pitch varying from 10 to 20 for Reynolds numbers range between 5000 and 50,000. It was found that the average friction factor and Nusselt number increased with increase in relative roughness height. The average Nusselt number of the roughened duct was about 2.10, 2.24 and 2.34 times than that of the smooth duct for relative roughness height of 0.020, 0.027 and 0.033 respectively. The average friction factor of the roughened duct was about 3.08, 3.67, and 4.26 times than that of the smooth duct. The increase in the average Nusselt number and average friction factor for relative roughness pitch of 10, 15 and 20 in the roughened duct was about 2.38, 2.14, 2.01 and 4.25, 3.39, 2.93 times than that of the smooth duct respectively.

Gupta et al. [49] studied effect of transverse wire roughness on heat and fluid flow characteristics for solar air heater ducts with an absorber plate having transverse wires fixed on the underside of it as shown in Fig. 7 for Reynolds number range of 3000–18,000, duct aspect ratio of 6.8–11.5, relative roughness height of 0.018–0.052 at a relative roughness pitch of 10 with a range of roughness Reynolds number between 5 and 70. It is found that Stanton number increased initially with an increase in Reynolds number up to 12,000 and registered a slight fall thereafter. Verma and Prasad [50] reported the effect of transverse wire roughness on heat and fluid flow characteristics for three rectangular solar air heater ducts; two were roughened collectors and one was a plane surface.

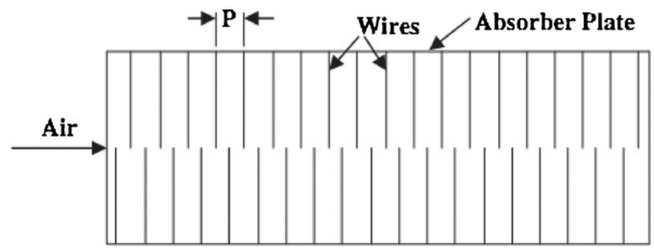


Fig. 8. Roughened absorber plate with transverse broken ribs.

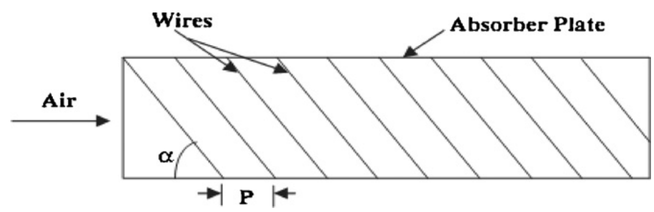


Fig. 9. Roughened absorber plate with inclined ribs.

Transverse wires were fixed on underside of absorber plate as shown in Fig. 7. Investigations were carried out for Reynolds number range of 5000–20,000 for high duct aspect ratio, relative roughness height of 0.01–0.03 at a relative roughness pitch of 10–40 and roughness Reynolds number range of 8–42. An optimum value of thermohydraulic performance of about 71% has been reported corresponding to roughness Reynolds number of 24.

5.1.2. Transverse broken ribs

The effect of broken transverse ribs on absorber plate of a solar air heater was studied by Sahu and Bhagoria [51]. Integral rib roughened absorber plates were prepared by fixing wires of 1.5 mm diameter over one side of absorber plate as shown in Fig. 8. Roughness geometry was having pitch (P) ranging from 10 to 30 mm, height of rib (e) was 1.5 mm and duct aspect ratio was 8. Investigated range of Reynolds number was 3000–12,000. Heat transfer coefficient enhancement over smooth duct was reported to be 1.25–1.4 times and maximum thermal efficiency of the order of 83.5% was obtained.

5.1.3. Inclined and V-shaped or discrete ribs

Gupta et al. [52] found optimum design parameters for outdoor condition of a roughened solar air heaters for varying relative roughness height (e/D) and for a relative roughness pitch (P/e) of 10 at an angle of attack (α) of 60°. Geometry of roughened absorber plate is shown in Fig. 9. An enhancement of heat transfer and friction factor was obtained of the order of 1.8 and 2.7 times respectively. Maximum heat transfer coefficient and friction factor values were obtained at an angle of attack of 60° respectively in the range of investigated parameters.

Muluwork et al. [53,54] compared thermal performance of roughened absorber plate fixed with staggered discrete V-apex (up and down) as shown in Fig. 10. It is reported that Stanton number increased with an increase of relative roughness length

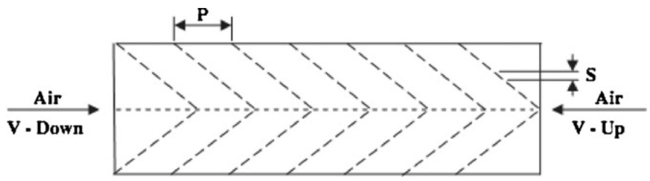


Fig. 10. Roughened absorber plate with discrete V shaped ribs up and downstream.

ratio in the range of 3–7. Reported Stanton number for V-down discrete ribs was higher than the corresponding V-up and transverse discrete roughened surfaces. Enhancement in Stanton number ratio was found to be of the order of 1.32–2.47.

Momin et al. [55] studied the effect of geometrical parameters on heat transfer and fluid flow characteristics of rectangular duct of solar air heater having V-shaped ribbed roughness on the absorber plate as shown in Fig. 11. This experimental investigation covered a Reynolds number range of 2500–18,000, relative roughness height (e/D) of 0.02–0.034 and angle of attack (α) of 30–90° for a fixed relative roughness pitch (P/e) of 10. It was reported that V-shape ribs with an angle of attack (α) of 60° enhanced Nusselt number by 1.14 and 2.30 times and friction factor by 2.30 and 2.83 times over inclined ribs and smooth plate respectively. Correlations for nusselt number and friction factor were developed.

Karwa [56] reported the effect of inclined discrete and continuous ribs on thermohydraulic performance of solar air heater for Reynolds number range of 2800–15,000, relative roughness height of 0.0467–0.050, fixed relative roughness pitch of 10 and duct aspect ratio of 7.19–7.75. Roughness geometries used in this study are shown in Fig. 12. Stanton number and friction factor correlations were developed. Enhancement in Stanton number and friction factor over smooth duct was observed of the order of 65–90% and 2.68–2.94 times respectively. It is reported that 60° inclined rectangular ribs produce better results than transverse ribs. It is also reported that enhancement in Stanton number over smooth duct is 102–137%, 110–147%, 93–134% and 102–142% for rib arrangement of V-up continuous, V-down continuous, V-up discrete and V-down discrete respectively.

Karmare and Tikekar [57] studied the heat transfer coefficient and friction factor characteristics of artificial roughened duct with metal grit ribs as shown in Fig. 13. Effect of range of system parameters of grit geometry on heat transfer coefficient and friction factor was investigated for Reynolds number range of 4000–17,000. It was found that plate having roughness parameters $l/s = 1.72$, $e/D = 0.044$ and $P/e = 17.5$ resulted optimum performance and as compared to smooth duct yields up to two-fold enhancement in Nusselt number and three-fold enhancement in friction factor.

Aharwal et al. [58] investigated effect of artificial roughness by using an inclined discrete rib arrangement in a rectangular duct shown in Fig. 14. Maximum enhancement in Nusselt number and friction factor as compared to smooth duct was observed to be 2.59 and 2.87 times respectively. Particle image velocimetry (PIV) system was used to visualise the effects of angle of inclination of ribs on the flow behaviour. Based on experimental results, correlations for nusselt number and friction factor were developed.

Varun et al. [59] studied heat transfer and friction characteristics by using a combination of inclined as well as transverse ribs as shown in Fig. 15 for Reynolds number range of 2000–14,000. It is reported that roughened absorber plate having relative roughness pitch (P/e) of 8 resulted in best performance.

Saini and Saini [60] studied the effect of arc shaped ribs on heat transfer and fluid flow characteristics of rectangular duct of solar air heater as shown in Fig. 16. This experimental investigation covered a Reynolds number range of 2000–17,000, relative roughness

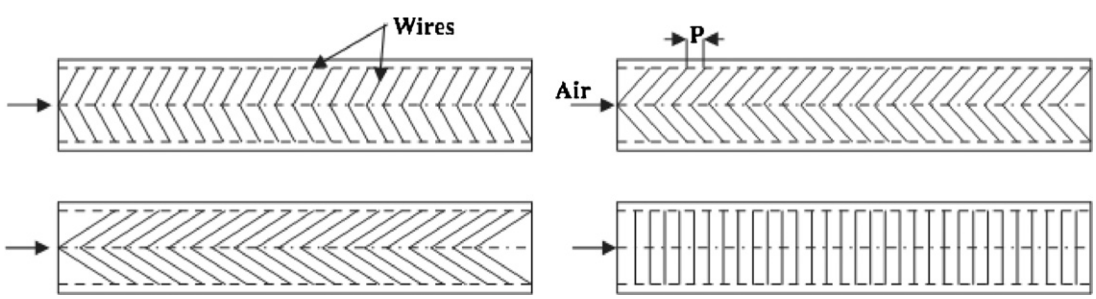


Fig. 11. Roughened absorber plate with V shaped and transverse ribs.

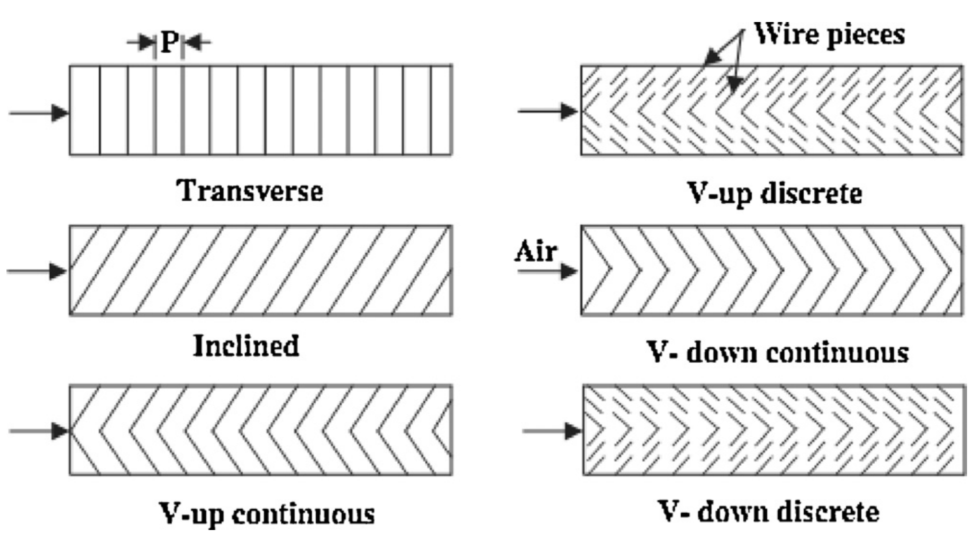


Fig. 12. Roughened absorber plate with transverse, inclined discrete and continuous ribs.

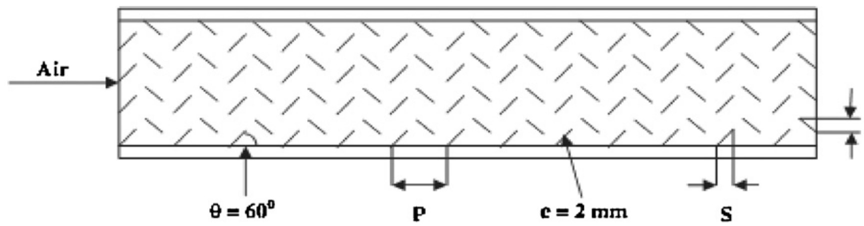


Fig. 13. Roughened absorber plate with metal grit ribs.

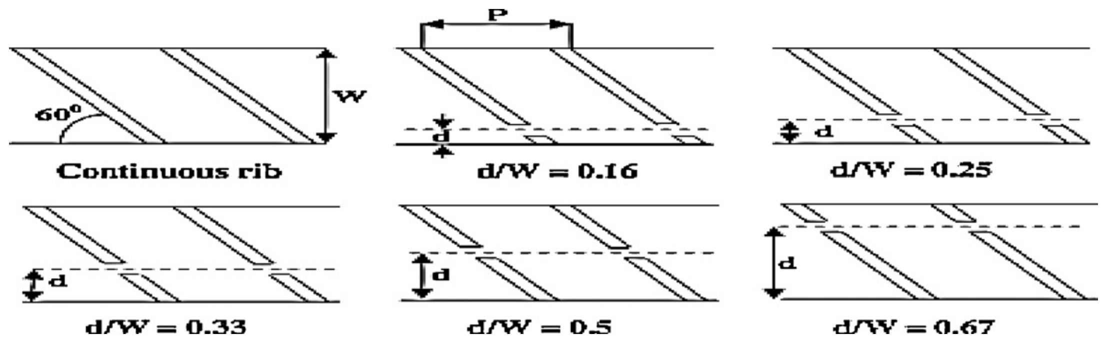


Fig. 14. Roughened absorber plate with inclined discrete ribs.

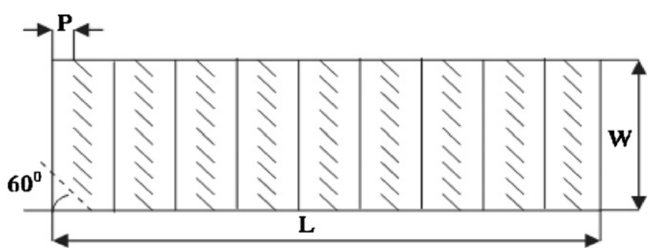


Fig. 15. Roughened plate with combined inclined and transverse ribs.

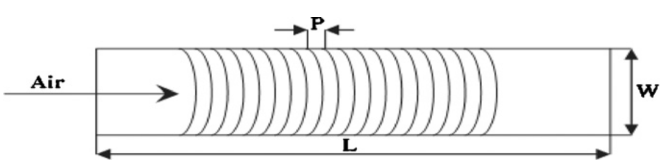


Fig. 16. Arc shaped rib roughness.

height (e/D) of 0.0213–0.0422 and relative angle of attack of flow ($\alpha/90$) of 0.3333–0.6666 for a fixed relative roughness pitch (P/e) of 10. Maximum enhancement in Nusselt number and friction factor as compared to smooth duct was observed to be 3.6 and 1.75 times respectively.

Hans et al. [61] carried out experimental investigation of a solar air heater duct with artificially roughened absorber plate in forms of multiple V-shaped ribs as shown in Fig. 17. Study showed that the maximum heat transfer enhancement occurred for relative roughness width (W/w) of 6 while friction factor was maximum at $W/w = 10$. Nusselt number is maximum corresponding to 60° angle of attack and for the relative pitch P/e of 8.

The heat and fluid flow characteristics of rectangular duct having its one broad wall heated and roughened with periodic 'discrete V-down rib' as shown in Fig. 18 were experimentally investigated by Singh et al. [62]. The result showed that the maximum increase in Nu and f over that of smooth duct was 3.04 and 3.11 folds respectively. The rib parameters corresponding to maximum increase in Nu and f were $d/w = 0.65$, $g/e = 1.0$, $P/e = 8.0$, $\alpha = 60°$ and $e/D_h = 0.043$.

5.2. Rib formation by machining process

Experimental investigations are reported in the literature to study heat transfer and friction characteristics by using integral ribs generated on absorber plate by machining process. Different shapes, sizes and orientation of ribs have been used to generate artificial roughness on absorber plate by this method as discussed in the following sections.

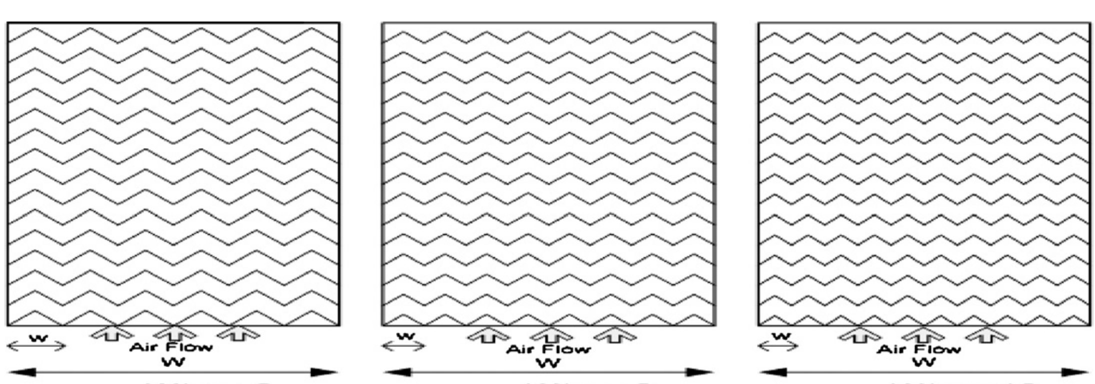


Fig. 17. Roughened plate with multiple V shaped rib roughness.

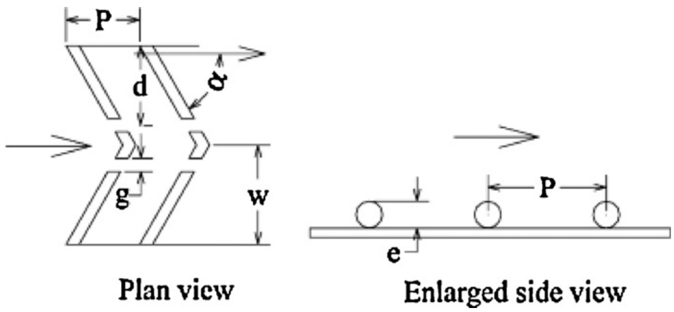


Fig. 18. Discrete V shaped rib roughness.

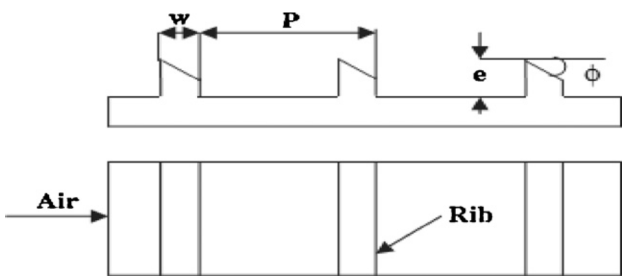


Fig. 19. Integral chamfered rib roughness on absorber plate.

5.2.1. Chamfered ribs

Karwa et al. [63] investigated integral chamfered ribs as artificial roughness as shown in Fig. 19. Experimental study was carried out by taking rib chamfer angles of −15°, 0°, 5°, 10°, 15° and 18° for a rectangular duct having aspect ratio of 4.8, 6.1, 7.8, 9.6 6 and 12 under a Reynolds numbers range of 3000–20,000. Range of relative roughness heights (e/D) and relative roughness pitch (P/e) was 0.0141–0.0328 and 4.5–8.5 respectively. In comparison to smooth duct, artificial roughened duct yielded up to about two and three times increase in the Stanton number and friction factor respectively.

5.2.2. Wedge shaped ribs

Bhagoria et al. [64] experimentally investigated heat transfer and friction factor characteristics of air heater rectangular duct roughened by wedge shaped transverse integral ribs as shown in Fig. 20 for Reynolds number range of 3000–18,000. Range of relative roughness height (e/D), relative roughness pitch (P/e) and rib wedge angle (f) was 0.015–0.033, $60.17\varphi^{-1.0264} < p/e < 12.12$ and 8–15° respectively. Authors reported an enhancement in Nusselt number and friction factor of the order of 2.4 and 5.3 times respectively as compared to smooth duct.

5.2.3. Combination of different integral rib roughness elements

Jaurker et al. [65] experimentally investigated on heat and fluid flow characteristics for fully developed turbulent flow in a rectangular duct having repeated integral transverse rib-groove roughness as shown in Fig. 21 for Reynolds number range of 3000–21,000. Enhancement of Nusselt number of the order of 2.75 times of the smooth duct and 1.57 times of ribbed duct with similar rib height and rib spacing was observed. Whereas ribbed duct with similar rib height and rib spacing provides Nusselt number values of the order of 1.7 times that of smooth duct for range of parameters. On the other hand friction factor increases in the order of 3.61 times that of smooth duct and 1.17 times that of ribbed duct. Whereas a ribbed duct with similar rib height and rib spacing results in friction factor value of the order of 3 times that of the smooth duct.

Layek et al. [66] investigated heat transfer and friction characteristics of repeated integral transverse chamfered rib-groove roughness as shown in Fig. 22 for a Reynolds number range of 3000–21,000, relative roughness pitch of 4.5–10, chamfer angle of 5–30°, relative groove position of 0.3–0.6 and relative roughness height of 0.022–0.04. Authors reported that Nusselt number and friction factor increased by 3.24 times and 3.78 times respectively as compared to smooth duct. Maximum enhancement of Nusselt number and friction factor was obtained corresponding to relative groove position of 0.4.

5.3. Wire mesh or expanded metal mesh ribs

Generation of artificial roughness on the absorber plate is considered to be a cumbersome task and may not be economically feasible for large scale production of solar air heaters for various applications. In order to solve this problem up to some extent, few experimental investigations based on wire mesh or expanded metal mesh as roughness element is reported in the literature.

Saini and Saini [67] used expanded metal mesh as roughness geometry and obtained an enhancement of heat transfer coefficient and friction factor of the order 4 and 5 times over the smooth duct corresponding to an angle of attack of 61.9° and 72° respectively. Roughness geometry investigated by Saini and Saini is shown in Fig. 23.

5.4. Dimple/protrusion shaped geometry

Generation of dimples/protrusions on surface of absorber plate is also considered to be a simple and economical methodology to create artificial roughness. It is a subject of many recent experimental investigations. Use of dimple shape roughness produced augmented surface heat transfer levels as compared to channels with smooth surfaces and at par with other artificial roughness geometries. On the other hand pressure drop or friction loss usually does not increase appreciably as compared to other rough channels.

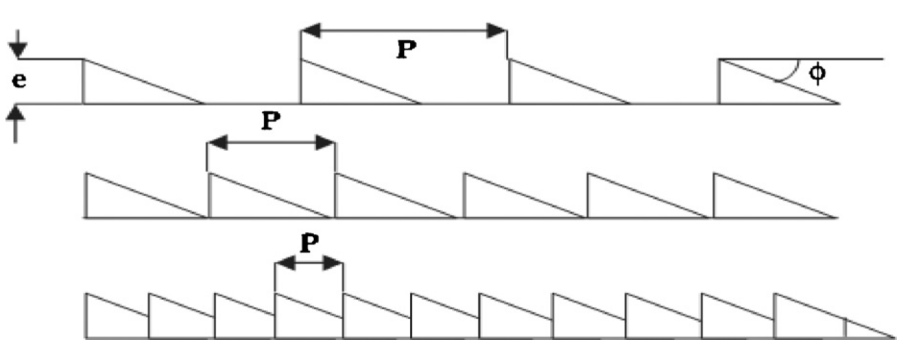


Fig. 20. Absorber plate having transverse wedge shaped rib roughness.

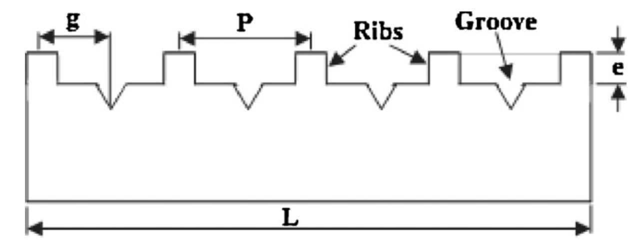


Fig. 21. Absorber plate having rib grooved roughness.

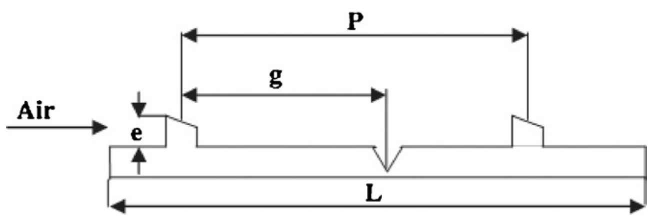


Fig. 22. Absorber plate having chamfered rib grooved roughness.

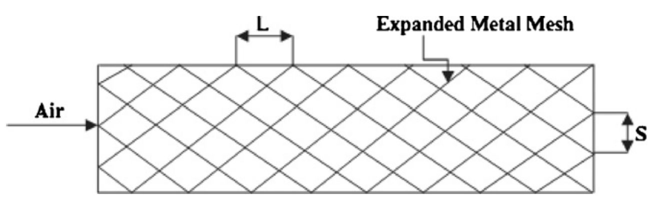


Fig. 23. Expanded metal mesh on absorber plate.

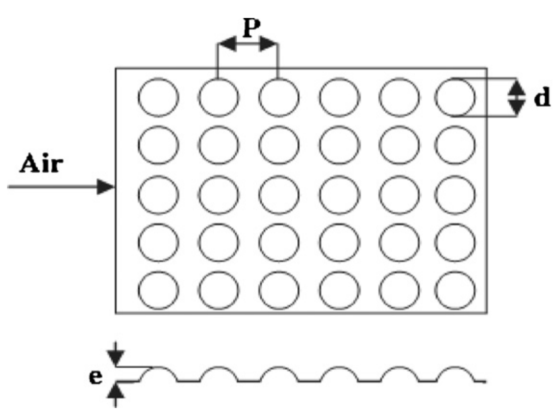


Fig. 24. Dimple shaped protrusion on absorber plate.

Saini and Verma [68] carried out an experimental investigation on fluid flow and heat transfer characteristics of solar air heater duct having dimple-shaped artificial roughness as shown in Fig. 24. The investigation covered the range of Reynolds number from 2000 to 12,000, relative roughness height from 0.018 to 0.037 and relative roughness pitch from 8 to 12. Maximum value of Nusselt number was found corresponding to relative roughness height of 0.0379 and relative roughness pitch of 10 and minimum value of friction factor was been found corresponding to relative roughness height of 0.0289 and relative roughness pitch of 10.

Bhushan and Singh [69] carried out an experimental investigation for a range of system and operating parameters to analyze the effect of artificial roughness on heat transfer and friction in solar air heater duct having protrusions as roughness geometry as shown in Fig. 25. The maximum enhancement of Nusselt number and friction factor was found 3.8 and 2.2 times respectively in comparison to smooth duct over the investigated range. Maximum enhancement in heat transfer coefficient was found to occur for relative short

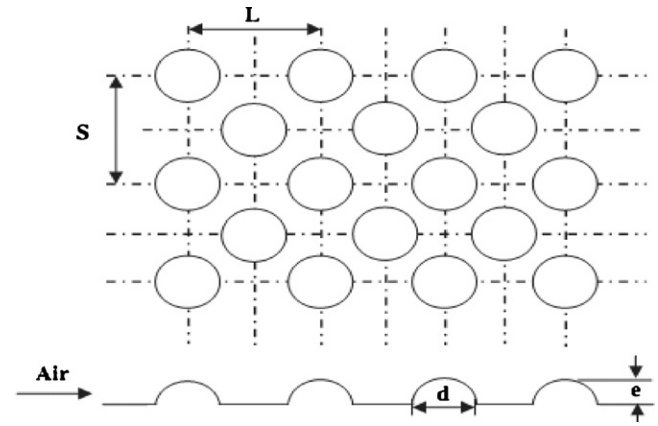


Fig. 25. Dimple protrusion in the staggered manner on absorber plate.

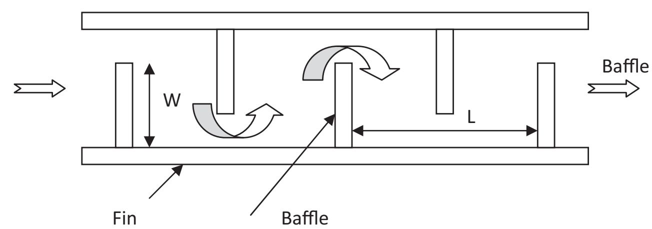


Fig. 26. Baffle attached to absorber plate.

way length (S/e) of 31.25, relative long way length (L/e) of 31.25 and relative print diameter (d/D) of 0.294.

6. Baffles

6.1. Solid baffles

The high thermal performance enhancement of heat exchanger systems in many industries is needed to use energy source efficiently. For decades, many engineering techniques have been developed for the rate of convective heat transfer from the channel surface. The uses of turbulators in the cooling channel or channel heat exchanger such as ribs, grooves or baffles are introduced in order to increase the convective heat transfer rate leading to the compact heat exchanger and increasing the efficiency. Periodic flow interruption by baffle arrays mounted periodically on the walls is an extensively used means for augmentation of heat transfer in many industrial applications. The baffles completely make the change of flow field and thus the distribution of local heat transfer coefficient. The baffle increases the degree of heat transfer coefficient and restarts the boundary layer after flow reattachment between baffles. The heat transfer increase is associated with increase in pressure drop due to increase in flow area effects. Thus the geometry parameters are the most important concern of design and the designers are looking towards the optimum parameters and geometry of baffles and their arrangements.

Yeh and Chou [70] experimentally investigate the efficiency of solar air heaters with baffles as shown in Fig. 26 and found considerable improvement in the collector efficiency of solar air heaters with fins in the collector are provided with attached baffles to create air turbulence and an extended heat transfer area and on increasing the density of baffles i.e. either increasing W/D_e or decreasing l/L also increases the collector efficiency but this will increase power consumption.

Yeh et al. [71] carried out theoretical investigation of the effect of collector aspect ratio on collector efficiency of baffled solar air heaters and found that with constant collector area, the collector

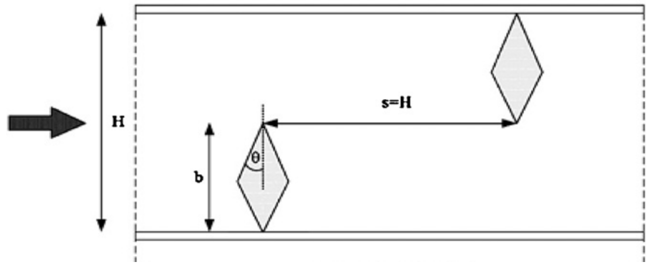


Fig. 27. Domain with staggered diamond shaped baffle.

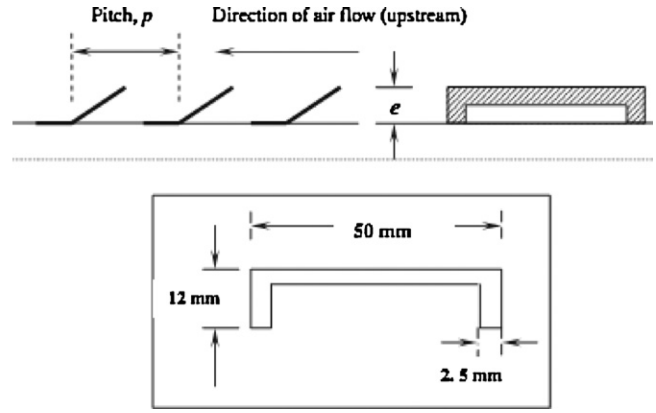


Fig. 28. Absorber plate with U shaped turbulators.

efficiency increases with increase in aspect ratio as on increasing the aspect ratio the cross-sectional area of the duct decreases and thus increase in the velocity of air flow and the convective heat transfer rate from absorber plate to flowing air. Mousavi and Hooman [72] numerically investigated the laminar fluid flow and heat transfer in the entrance region of a two dimensional horizontal channel with isothermal walls and with staggered baffles. It was observed that the Reynolds number is influential on the location of the periodically fully developed condition, as well as the blockage ratio. The two parameters affect the development in such a way that increasing any of the two will postpone the development and consequently increase the Nusselt number since the flow reattachment to the channel wall causes the washing of the wall and, hence, results in greater values of the local Nusselt number. However, it is shown that the concept of periodically fully developed ones does not necessarily mean the same as what we expected for a smooth channel, i.e., a region in which the Nusselt number will no longer change as the flow moves downstream. Romdhane [73] studied the solar collectors and gave a comparative study on various techniques favorise and increase the heat transfer coefficient between the caloporting fluid(air) and the absorber, the manner in which the air flows the absorber, the shape of the collector itself and those of inlets and outlets. It was found that on introduction of suitable baffles in solar air collectors increases the couple efficiency-increase in temperature. The baffles placed in the air channel situated between the insulator and the absorber, have the particularity of extending the trajectory of the circulation, to keep the caloporting air constantly in contact with the absorber, and finally to play the role of wings and improving the heat transfer from the absorber to the caloporting air. Sripattanapipat and Promvonge [74] carried out numerical investigation of laminar periodic flow and heat transfer in a two dimensional horizontal channel with isothermal walls and with staggered diamond shaped baffles as shown in Fig. 27. It was found that performance of laminar heat transfer in a channel fitted with two transverse staggered diamond baffles is obtained using numerical simulation. The order of enhancement is about 200–680% for using the diamond baffles and the augmentation is associated with enlarged friction loss ranging from 20 to 220 times above the smooth channel. The effect of interaction of the vortices induced by both types of baffles is numerically investigated and the enhancement of heat transfer for 5° diamond shaped baffle is around 6% higher than that of flat baffle.

Nie et al. [75] conducted numerical simulations of three-dimensional laminar forced convection flow adjacent to backward-facing step in rectangular duct to examine effects of the baffle on flow and heat transfer distributions. The step height is maintained as constant. A baffle is mounted onto the upper wall and its distance from the backward-facing step is varied. It was observed that baffle mounted onto the upper wall increases the magnitude of maximum Nusselt number at the stepped wall. One segment of the x_u-line developing close to the backward-facing step becomes shorter with decrease of the distance of the baffle from the backward-facing step. It becomes more relatively uniform in the spanwise direction as the distance of the baffle from the backward-facing step decrease. The other segment developing adjacent to the sidewall moves further downstream as the baffle moves in the stream wise direction away from the backward-facing step and the maximum Nusselt number on the stepped wall develops near the sidewall, and it moves further downstream as the location of the baffle moves in the stream wise direction. The friction coefficient at the stepped wall decreases as the distance of the baffle from the inlet increases. Bopche and Tandale [76] carried out experimental investigation to study heat transfer and friction factor by using artificial roughness by using U shaped turbulators on the absorber surface as shown in Fig. 28 of an air heater duct over the range of parameters Re: 3800–18,000, e/D_h = 0.0186–0.03986, p/e = 6.67–57.14, α = 90°. It was observed that Roughness pitch strongly affects the flow pattern and hence the performance of the duct. The turbulators geometry shows appreciable heat transfer enhancement even at low Reynolds number too Re < 5000 where ribs are inefficient. At Reynolds number Re = 3800, the maximum enhancement in Nusselt number and friction factor are of the order of 2.388 and 2.50 respectively and the maximum enhancement in Nusselt number and friction factor values compared to smooth duct are of the order of 2.82 and 3.72 respectively

Promvonge [77] carried out experimental investigation of heat transfer and friction factor characteristics of a rectangular duct of AR = 10 with multiple 60° V baffles as shown in Fig. 29 and the range of parameters investigated are e/H = 0.10, 0.20, 0.30, P/H = 1–3, Re: 5000–25,000. It was found that Nusselt number augmentation tends to increase with the rise of Reynolds number. The use of V baffles with e/H = 0.30 causes a very high heat transfer and pressure drop increase as compared with outer flow blockage ratios. In similar e/H it is clear that V baffles with PR = 1 give much higher heat transfer rate and friction factor than with PR = 2 and 3. For comparison in terms of thermal enhance factor, the use of V baffle with e/H = 0.10 leads to the highest value and is about 1.87 at PR = 1 and the lowest value of Reynolds number.

Promvonge et al. [78] carried numerical investigation on periodic laminar flow and heat transfer behaviors in a three dimensional isothermal wall square channel fitted with 30° angled baffles on two opposite channel walls and the range of parameters investigated are Re: 100–2000, PR = 1, 1.5, 2, BR = 0.1, 0.15, 0.2, 0.25, 0.3. Heat transfer enhancement is found about 1.2–11 times for using the 30 baffle pair with BR = 0.1–0.3 and PR = 1, 1.5 and 2. However, the heat transfer augmentation is associated with enlarged pressure loss ranging from 2 to 54 times above the smooth channel depending on the BR, PR and Re values. Thermal enhancement factor for the 30 inline baffle is found to be much higher than unity and its maximum value is about 4.0 at the highest Re and PR = 2 indicating higher thermal performance over the smooth channel. When effect of the baffle PR and BR values on heat transfer rate

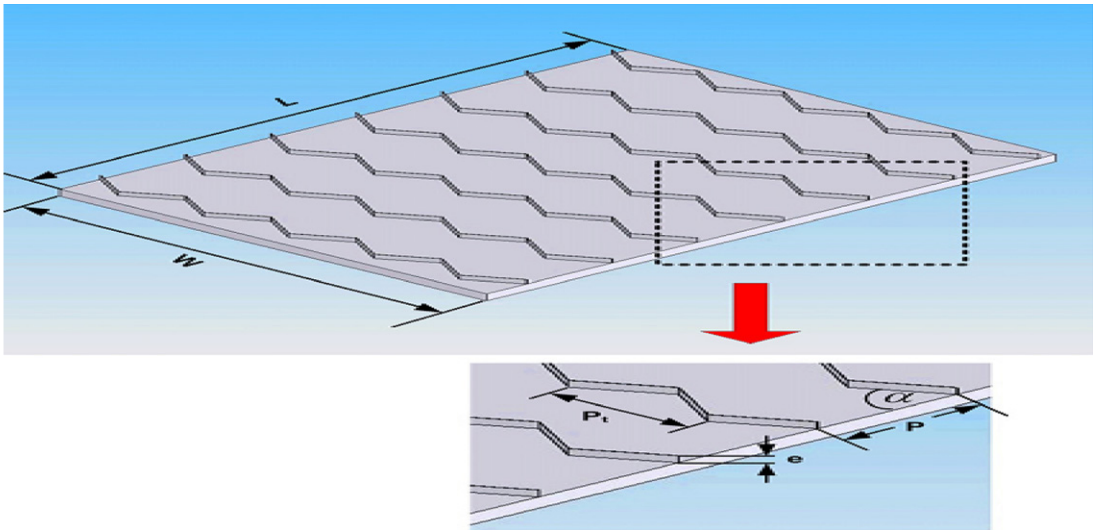


Fig. 29. Multiple 60° V shaped baffle roughned plate.

is examined, it is found that the maximum enhancement factor is about 4.0 for BR = 0.15, PR = 2.0 and Re = 2000. Kwankaomeng and Promvonge [79] carried numerical investigation on periodic laminar flow and heat transfer behaviors in a three dimensional isothermal wall square channel fitted with 30° angled baffles on one channel wall and the range of parameters investigated are Re: 100–2000, PR = 1, 1.5, 2, BR = 0.1–0.5 and heat transfer enhancement was found about 1.00–9.23 times for using the baffle with BR = 0.1–0.5. However, the heat transfer augmentation is associated with enlarged pressure loss ranging from 1.09 to 45.31 times above the smooth duct. Thermal enhancement factor for the angled baffle is much higher than unity and its maximum value is about 3.1 at BR = 0.3 and PR = 1.5, indicating higher thermal performance over the smooth duct. Promvonge and Kwankaomeng [80] carried out numerical investigation to examine laminar flow and heat transfer characteristics in a three dimensional isothermal wall square channel with 45° staggered angled baffles with range of Reynolds in the range of 100–1200. It was found that the P vortex flow created by using the 45° baffles helps to induce impingement flows on the BLE side wall and wall in the baffle cavity leading to drastic increase in heat transfer in the square channel. The order of enhancement is about 100–1100% for using both the 45° baffles with BR = 0.05–0.3 and the heat transfer augmentation is associated with enlarged pressure loss ranging from 2 to 90 times above the smooth channel. Thermal enhancement factors for both the 45° baffle arrays are found to be almost the same for BR ≤ 0.20 and much higher than unity and their maximum values are about 2.6–2.75 indicating higher thermal performance over the smooth channel.

6.2. Porous/perforated baffles

Roughness elements of larger height give a high increase in the heat transfer but increase in pressure drop is a serious concern. Hot zones develop in the wake of these elements because of recirculating flow. This leads to lower heat transfer from these zones; thus an attempt has been made by the designers to overcome this effect by putting perforation in the baffles which increase the heat transfer from these zones and help in reducing the pressure drop across the channel. The perforated elements allow a part of the flow to pass through these perforations and thus the hot zones and form drag are reduced. Solar air heater can be modeled as an asymmetrically heated high aspect ratio rectangular duct with flow regime ranging from laminar to early turbulent (Re: 1000–15,000). Due to the asymmetric heating, the thermal boundary layer in the laminar regime develops such that the air temperature decreases nearly monotonously from the heated absorber plate to the lower insulated side of the duct. In the turbulent regime, most of the temperature drop occurs through the laminar sublayer at the heated wall. The transitional flow, which is of main interest in the solar air heaters, can be regarded as a mix of the laminar and turbulent flows. Furthermore, for the gases, unlike the liquid metals, resistance to the heat transfer extends up to the buffer layer (the layer between the laminar sublayer and turbulent core). Therefore, the elements projecting beyond the sublayer must help. Yang and Hwang [81] carried out numerical predictions on the turbulent fluid flow and heat transfer characteristics for rectangular channel with porous baffles which are arranged on the bottom and top channel walls in a periodically staggered manner. It was found that when the solid type baffles are replaced by the porous type baffles, reducing the effect thermal conductivity of the baffle, increasing of heat transfer surface and changing the flow transport phenomena. Ko and Anand [82] carried out experimental investigation to measure module average heat transfer coefficients in uniformly heated rectangular channel with wall mounted porous baffles as shown in Fig. 30. The results show that the flow and heat transfer to reach periodically fully developed state downstream of the seventh module. The heat transfer enhancement ratio decreases with increase in Reynolds number and increases with increasing pore density. The heat transfer enhancement ratio reaches a maximum value of 300% for the range of parameters. The heat transfer enhancement ratio is found to be higher for taller ($B_h/D_h = 2/3$) and thicker ($B_t/D_h = 1/3$) baffles.

Tzeng et al. [83] carried out experimental determination of local and average heat transfer characteristics in asymmetrically heated sintered porous channels with metallic baffles. The fluid medium was air. Measurements on the test specimen of four modes, without baffles (A), with periodic baffles on the top portion (B), with periodic baffles on the bottom portion (C) and with staggered periodic baffles on both sides (D), are performed. It was observed that at a given heat flux, the wall temperature increased with the axial distance, and declined as the Reynolds number increased. Additionally, when baffles were attached on the heated wall (as in modes B and D), the wall temperatures measured at the baffles were slightly lower than those at the nearby points, especially at large Reynolds numbers. Molki and Mostoufizadeh [84] carried out an experimental investigation of heat transfer and pressure drop in a rectangular duct with repeated baffle blockages and the baffles are arranged in a staggered fashion with fixed axial spacing. It

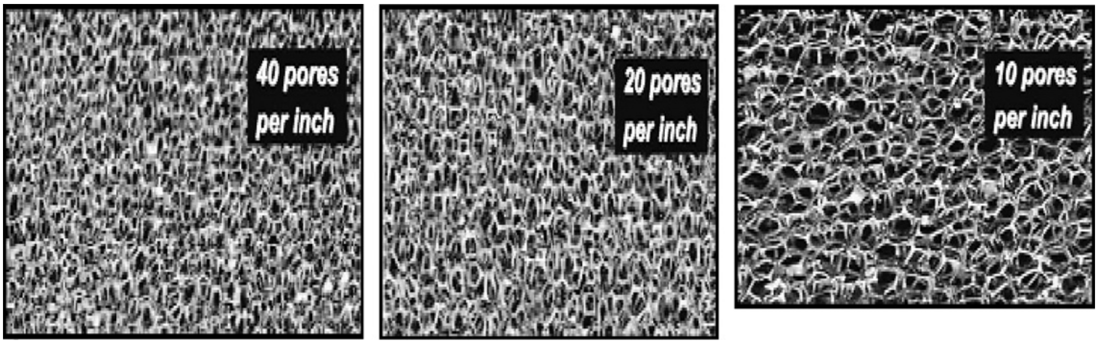


Fig. 30. Aluminum foam structure.

was found that baffle affects the entrance length of the duct, and the entrance length decreases monotonically with an increase in baffle height. The mass transfer and pressure data were combined under the equal pumping power condition, and enhancements of up to 90% occurred for the smallest baffle. Hwang and Liou [85] investigated experimentally the effect of perforated ribs on turbulent heat transfer and friction in a rectangular channel with perforated ribs with an open area ratio of 50% are staggered on two opposite walls of the channel. Four rib pitch to height ratios 5, 10, 15, 20 and two rib height to channel hydraulic diameter ratios 0.081 and 0.169 are examined and the range of Reynolds number is taken from 10,000 to 50,000. It was found that perforated rib geometry has Nusselt number and friction factor about 115% and 60%; then solid ribs over the investigated range and the slightly higher heat transfer coefficient and significantly lower pressure drop accompanying the perforated rib reflect a higher thermal performance. Hwang et al. [86] experimentally investigated the effect of fence thickness on pressure drop and heat transfer in a perforated fence channel. It was found that the fence thickness strongly affects the thermal performance through influencing the fence permeability limit, and the permeability limit of the perforated fence decreases with the decrease of the fence thickness to height ratio. Liou and Chen [87] studied periodically turbulent heat transfer and friction in a rectangular passage of aspect ratio 4 with perforated rectangular ribs detached from one wall using laser holographic interferometry, smoke-streak flow visualization; pressure probing and laser-Doppler Velocimetry measurements were performed to illustrate the local Nusselt number distribution and range of parameters investigated $H/D_e = 0.081$, 0.106, 0.162, Re = 5000–50,000, $p/e = 10$. It was found that for the range of parameters investigated the thermal performance of Nu_p detached perforated ribs are as high as 1.3–1.9 times than that of smooth duct at same pumping power and a maximum Nu_p/Nu_s for middle values of $H/D_e = 0.106$ in the lower Reynolds number and a Nu_p/Nu_s is independent of H/D_e for high range of Reynolds number. Li and Kottke [88] experimentally investigated the local heat transfer and pressure drop on the shell side of shell and tube heat exchangers with segmental baffles for different baffle spacing and found that an increasing baffle spacing can increase the heat transfer coefficient in the whole baffle compartment both due to reduction of the percentage of the leakage stream and due to the higher flow velocity through the baffle opening. The pressure drop coefficient for long baffle spacing is higher than for a short one. Dutta and Dutta [89] experimentally investigated the frictional loss and heat transfer behavior of turbulent flow in a rectangular channel with isoflux heating from the upper surface for different sizes, positions and orientation of inclined baffles attached to the heated surface and found both average and local Nusselt numbers are significantly dependent on the baffle plate orientation and the Nusselt number ratio decreases as the plate is placed at a more streamlined position. The friction factor ratio decreases with a decrease in the angle of baffle and also with an increase in the perforation density. Moreover friction factor ratio increases with an increase in the average Nusselt number ratio for a given configuration. Dutta and Hossain [90] experimentally investigated the local heat transfer characteristics and the associated frictional head loss in a rectangular channel with inclined solid and perforated baffles and found that the overall heat transfer coefficient is much higher with two inclined baffles than that with a single baffle placed in the same channel. The average Nusselt number can be as high as 5 times the average Nusselt number of a smooth channel. Karwa et al. [91] experimentally investigate the heat transfer and friction in rectangular ducts with transverse baffles solid or perforated as shown in Fig. 31 attached to one broad wall and range of parameters investigated are P/e: 29, e/H: 0.495 and Re: 2850–11,500 and study reveals the enhancement of 73.7–82.7% in Nusselt number over smooth duct for solid baffles and from 60.6–62.9% to 45–49.7% for the perforated baffles and friction factor for the solid baffles is found to be 9.6–11.1 times of the smooth duct.

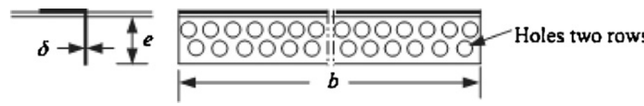


Fig. 31. Transverse perforated baffle with two rows of holes.

Lin [92] experimentally investigates the local heat transfer in rectangular channel with baffles, and analyzes the experimental results of baffles with different heights and pores in the range of Reynolds number and three heating quantities with the range of parameters H: 10–50 mm, N: 1–3, Q: 40–100 l/min, Re: 702–1752 and Q: 90–750 W/m^2. It was found that the maximum Nusselt number without baffles of pores is generated at $q_{in} = 750\,W/m^2$, Re = 1752 at $X/L = 0.04$. The distribution of Nusselt number declines gradually with the increase of X/L and its minimum value is generated at $X/L = 0.2$, with the difference of Nusselt number approx 50% and a single pore baffle has a highest average Nusselt number, higher than that of two and three pores baffles by 26 and 28, up to 25% and 27% respectively. Huang et al. [93] studied the detailed measurement of local heat transfer coefficients in a square channel with a perforation baffle by using transient liquid crystal thermography with the parameters of investigation are Reynolds number, the baffle height, and the hole numbers on the perforation baffles. It was found that heat transfer coefficients off center are better than those in center at downstream of the baffle. It is resulted from two secondary flows that appeared off center after the air flow passes through the baffle and the heat transfer enhancement in case of a baffle with holes is greater than that without holes. Karwa and Maheshwari [94] carried out experimental study of heat transfer and friction in a rectangular section duct with transverse fully perforated baffles (open area ratio of 46.8%) as shown in Fig. 32 and half perforated baffles (open area ratio of 26%) affixed to one of the

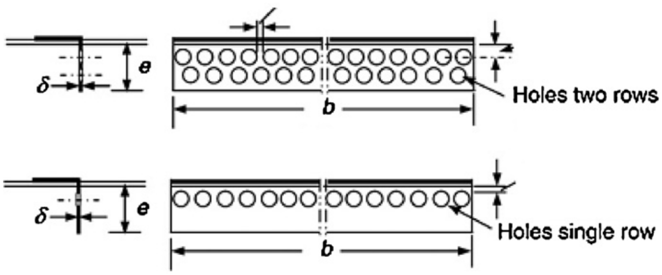


Fig. 32. Transverse perforated baffle with double and single rows of hole.

wall over the range of P/e: 7.2–28.8 and Re: 2700–11,150. Enhancement of 79–169% in Nusselt number was reported over the smooth duct for fully perforated baffles and 133–274% for the half perforated baffles while the friction factor for the fully perforated baffles is 2.98–8.02 times of that for smooth duct and is 4.42–17.5 times for the half perforated baffles.

7. Delta winglet

Swirl/vortex generators are inserted into the forced flow that creates secondary flow or rotary flow and used in augmentative heat transfer in many engineering applications to enhance the rate of the heat and mass transfer equipment including heat exchanger, vortex combustor, drying process, etc. Vortex generators are in the form of wings or winglets. These vortex generators are of triangular or rectangular shapes which can be welded or punched and bend out of the plate so that they project into the flow with an angle of attack to the main flow direction. If the trailing edge is attached to the plate it is termed as a wing and when the chord length is attached to the plate then it is called a winglet. The different geometries of the vortex generators are shown in Fig. 33. These vortex generators induce longitudinal stream-wise vortices in the flow field. The vortices develop along the edge of the vortex generator due to the pressure difference between the front surface facing the flow and the back surface. These vortices are called longitudinal vortices because their axes of rotation are aligned to the direction of main flow. Heat transfer enhancement by winglet type vortex generators mounted at the leading edge of a flat plate was found to be about 50–60% improvement in average heat transfer over the surface of the plate Gentry and Jacobi [96].

Torii et al. [97] used a novel technique that can augment heat transfer but nevertheless can reduce pressure-loss in a fin-tube heat exchanger with circular tubes in a relatively low Reynolds number flow, by deploying delta winglet-type vortex generators. The winglets are placed with a heretofore unused orientation for the purpose of augmentation of heat transfer. This orientation is called as "common flow up" configuration as shown in Fig. 34. The proposed configuration causes significant separation delay, reduces form drag, and removes the zone of poor heat transfer from the near-wake of the tubes. This enhancement strategy has been successfully verified by experiments in the proposed configuration. In case of staggered tube banks, the heat transfer was augmented by 30–10%, and yet the pressure loss was reduced by 55–34% for the Reynolds number (based on two times channel height) ranging from 350 to 2100, when the present winglets were added. In case of in-line tube banks, these were found to be 20–10% augmentation, and 15–8% reduction, respectively.

An experimental study was carried out by Yakut et al. [98] for tapes with double-sided delta-winglets under different geometrical and flow parameters, including angles of attack (90°, 60° and 30°), winglet heights (8, 12 and 16 mm), pitch arrangements (25, 50 and 75 mm) and Reynolds numbers (3690, 10,493 and 16,906). By using the Taguchi experimental-design method, the optimum parameters of the turbulator were determined by obtaining the Nusselt number, friction factor, amplitude of fluctuation pressure of the vortices and the vortex-shedding frequency. The optimum results were obtained at a Reynolds number of 16,906, 25 mm pitch,

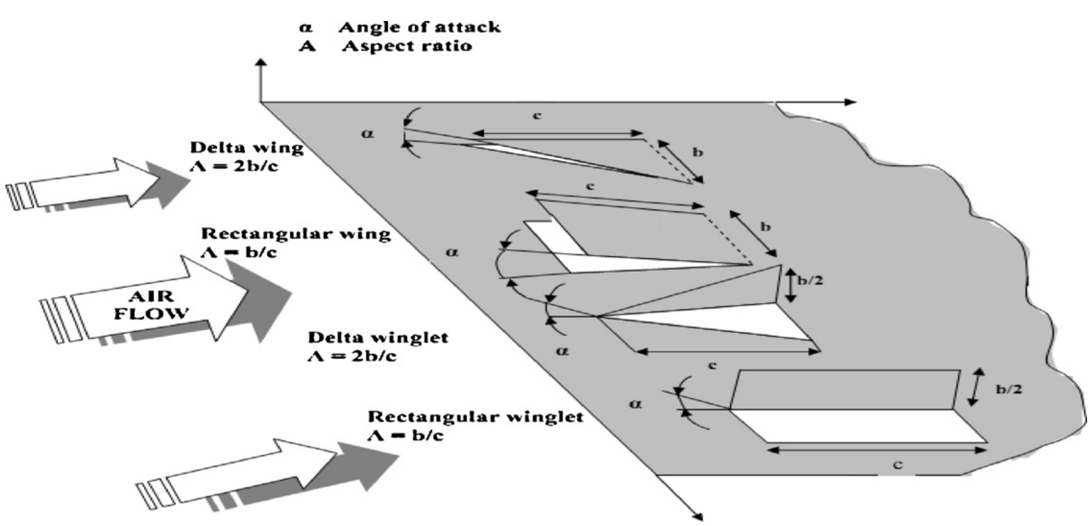


Fig. 33. Longitudinal vortex generators.

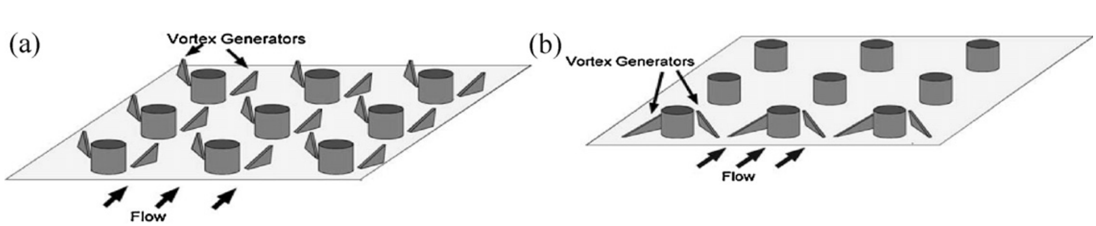


Fig. 34. Configuration of winglet type vortex generator on the fin surface-tube bank: (a) "common flow down" configuration; (b) "common flow up" configuration.

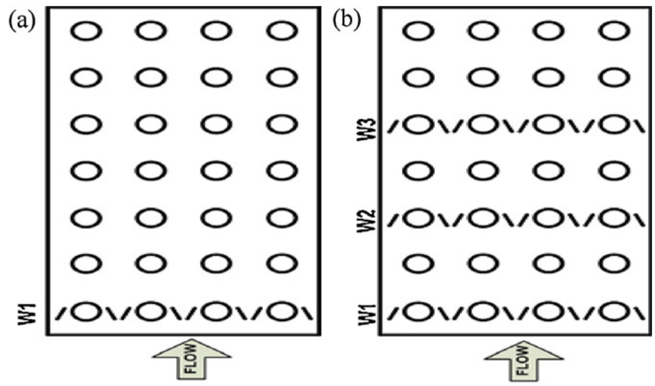


Fig. 35. (a) Single row; (b) three row inline array configurations.

8 mm height of winglet and 30° angle of attack. For lower frequencies, optimum conditions occurred at a Reynolds number of 16,906 for 75 mm pitch, 8 mm height of winglet and 60° angle of attack. The potential of winglet type vortex generator (VG) arrays for air-side heat transfer enhancement is experimentally evaluated by full scale wind-tunnel testing of a compact plain-fin-and-tube heat exchanger by Joardar and Jacobi [99]. The effectiveness of a 3VG alternate-tube inline array of vortex generators as shown in Fig. 35 is compared to a single row vortex generator design and the baseline configuration. The winglets are placed in a common flow-up orientation for improved tube wake management. The overall heat transfer and pressure drop performance are assessed under dry-surface conditions over a Reynolds number range based on hydraulic diameter of $220 \leq Re \leq 960$. It is found that the air-side heat transfer coefficient increases from 16.5% to 44% for the single-row winglet arrangement with an increase in pressure drop of less than 12%. For the three-row vortex generator array, the enhancement in heat transfer coefficient increases with Reynolds number from 29.9% to 68.8% with a pressure drop penalty from 26% at Re = 960 to 87.5% at Re = 220.

A numerical investigation is carried out by Tian et al. [100] to study the air-side heat transfer and fluid flow characteristics of wavy fin-and-tube heat exchanger with delta winglets. The wavy fin-and-tube heat exchangers which have three-row round tubes in staggered or in-line arrangements are studied. The numerical results show that each delta winglet generates a down-stream main vortex and a corner vortex. For the in-line array, the longitudinal vortices enhance the heat transfer not only on the fin surface in the tube wake region but also on the tube surface downstream of the delta winglet; for the staggered array, longitudinal vortices are disrupted at the first wavy trough downstream from the delta winglet and only develop a short distance along the main-flow direction, and the vortices mainly enhance the heat transfer of the fin surface in the tube wake region. The longitudinal vortices generated by delta winglet cause considerable augmentation of heat transfer performance for wavy fin-and-tube heat exchanger with modest pressure drop penalty. When $Re_{Dc} = 3000$, compared with the wavy fin, the j and f factors of the wavy fin with delta winglets in staggered and in-line arrays are increased by 13.1%, 7.0% and 15.4%, 10.5%, respectively. Min et al. [101] develop a modified rectangular longitudinal vortex generator (LVG) as shown in Fig. 36 obtained by cutting off the four corners of a rectangular wing and study fluid flow and heat transfer characteristics of this LVG mounted in rectangular channel experimentally and compared with those of original rectangular LVG. Results reveal that the modified rectangular wing pairs (MRWPs) have better flow and heat transfer characteristics than those of rectangular wing pair (RWP). Near the positions of $z = \pm 40$ mm from the center-line of the heater plate, the local heat transfer is enhanced due to the strong longitudinal vortices generated by the presence of the LVGs. The down-sweep of the longitudinal vortices is beneficial to the heat transfer enhancement. The distance from the core of the main vortices of MRWP1 to the heater wall is slightly lower than those of RWP, and hence MRWP1 has a comparably better heat transfer characteristic.

A second law analysis was carried out by Kotcioglu et al. [102] of a cross flow heat exchanger. The entropy generation in a cross flow HX with a new winglet-type convergent–divergent longitudinal vortex generator (CDLVG) is investigated. Optimization of HX channel geometry and effect of design parameters regarding the overall system performance are presented. For the HX flow lengths and CDLVGs the optimization model was developed on the basis of the entropy generation minimization (EGM). It was found that increasing the cross-flow fluid velocity enhances the heat transfer rate and reduces the heat transfer irreversibility. The test results demonstrate that the CDLVGs are potential candidate procedure to improve the disorderly mixing in channel flow of the cross-flow type HX for large values of the Reynolds number.

Heat transfer, flow friction and thermal performance factor characteristics in a tube fitted with delta-winglet twisted tape, using water as working fluid are investigated experimentally by Eiamsa-ard et al. [103]. Influence of the oblique delta-winglet twisted tape (O-DWT) and straight delta-winglet twisted tape (S-DWT) arrangements are also studied. The experiments are conducted using the tapes with three twist ratios ($y/w = 3$, 4 and 5) and three depth of wing cut ratios ($DR = d/w = 0.11$, 0.21 and 0.32) over a Reynolds number range of 3000–27,000 in a uniform wall heat flux tube. The results show that mean Nusselt number and mean friction factor in the tube with the delta-winglet twisted tape increase with decreasing twisted ratio (y/w) and increasing depth of wing

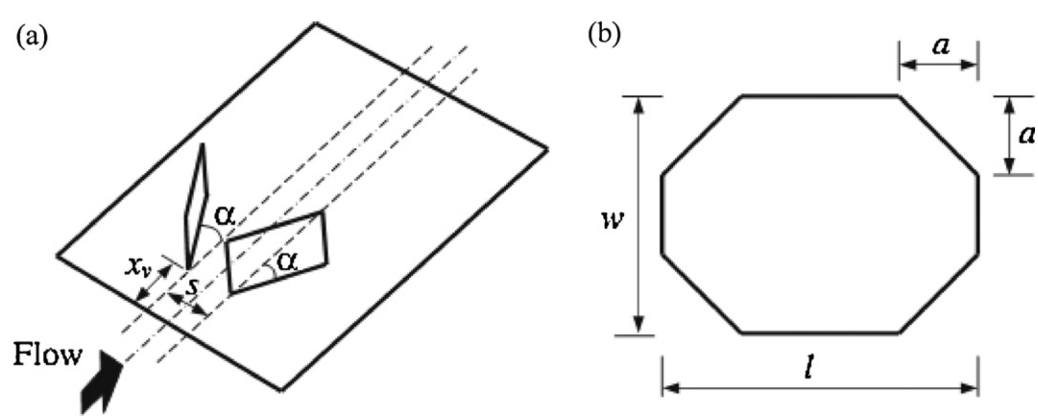


Fig. 36. Schematic view of present modified longitudinal vortex generator: (a) layout of common flow-down wings; (b) modified rectangular wing.

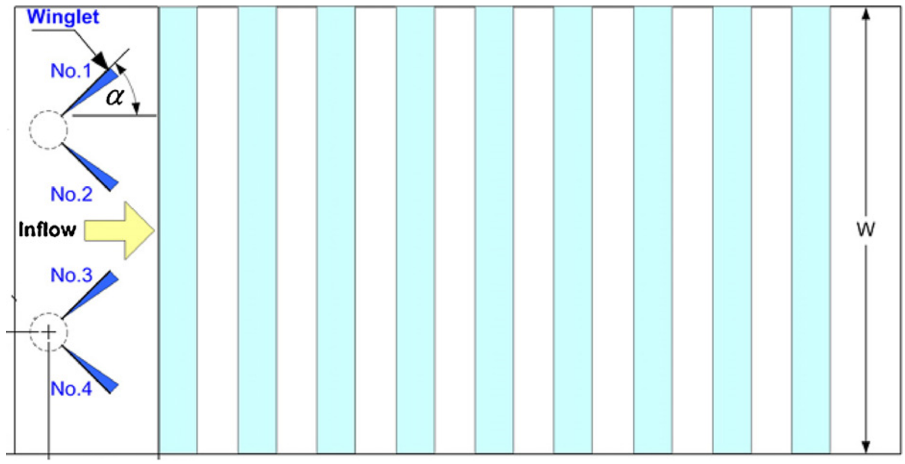


Fig. 37. Test section with winglet geometry.

cut ratio (DR). It was observed that the O-DWT is a more effective turbulator giving higher heat transfer coefficient than the S-DWT. Over the range considered, Nusselt number, friction factor and thermal performance factor in a tube with the O-DWT are, respectively, 1.04–1.64, 1.09–1.95, and 1.05–1.13 times of those in the tube with typical twisted tape (TT). An experimental investigation has been carried out by Chompookham et al. [104] to study the effect of combined wedge ribs and winglet type vortex generators (WVGs) on heat transfer and friction loss behaviors for turbulent air flow through a constant heat flux channel. To create a reverse flow in the channel, two types of wedge (right-triangle) ribs are introduced: wedge ribs pointing downstream and pointing upstream as shown in Fig. 37. The arrangements of both rib types placed inside the opposite channel walls are in-line and staggered arrays. To generate longitudinal vortex flows through the tested section, two pairs of the WVGs with the attack angle of 60° are mounted on the test channel entrance. The test channel has an aspect ratio, AR = 10 and height, H = 30 mm with a rib height, e/H = 0.2 and rib pitch, P/H = 1.33. The flow rate in terms of Reynolds numbers is based on the inlet hydraulic diameter of the channel ranging from 5000 to 22,000. The presence of the combined ribs and the WVGs shows the significant increase in heat transfer rate and friction loss over the smooth channel. The Nusselt number and friction factor values obtained from combined the ribs and the WVGs are found to be much higher than those from the ribs/WVGs alone. In conjunction with the WVGs, the in-line wedge pointing downstream provides the highest increase in both the heat transfer rate and the friction factor while the staggered wedge pointing upstream yields the best thermal performance.

Effects of combined ribs and delta-winglet type vortex generators (DWs) on forced convection heat transfer and friction loss behaviors for turbulent air flow through a solar air heater channel are experimentally investigated by Promvonge et al. [105]. The flow rate is presented in the form of Reynolds numbers based on the inlet hydraulic diameter of the channel ranging from 5000 to 22,000. The cross-section shape of the rib placed on the absorber plate to create a reverse flow is an isosceles triangle with a single rib height, e/H = 0.2 and rib pitch, Pl/H = 1.33. Ten pairs of the DW with its height, b/H = 0.4, transverse pitch, Pt/H = 1 and three attack angles (α) of 60°, 45° and 30° are introduced and mounted on the lower plate entrance of the tested channel to generate longitudinal vortex flow. The experimental results show that the Nusselt number and friction factor values for combined rib and DW are found to be much higher than those for the rib/DW alone. The larger attack angle of the DW leads to higher heat transfer and friction loss than the lower one. In common with the rib, the DW pointing upstream (PU-DW) is found to give higher heat transfer rate and friction loss than the DW pointing downstream (PD-DW) at a similar operating condition. In comparison, the largest attack angle (α = 60°) of the PU-DW yields the highest increase in both the Nusselt number and friction factor while the lowest attack angle of the PD-DW provides the best thermal performance. The performance of a pair of new vortex generators – curved trapezoidal winglet (CTW) has been experimentally investigated by Zhou and Ye [106] and compared its results with traditional vortex generators-rectangular winglet, trapezoidal winglet as shown in Fig. 38 and delta winglet using dimensionless factors j/j_0, f/f_0 and $R = (j/j_0)/(f/f_0)$. The results showed that delta winglet pair is the best in laminar and transitional flow region, while curved trapezoidal winglet pair (CTWP) has the best thermohydraulic performance in fully turbulent region due to the streamlined configuration and then the low pressure drop, which indicates the advantages of using this kind of vortex generators for heat transfer enhancement. Parametric study on CT WP showed that smaller attack angle (β = 0° and 15°), larger curvature (b/a = 1/2) and larger angle of inclination (α = 20°) gives better thermohydraulic performance under the present conditions.

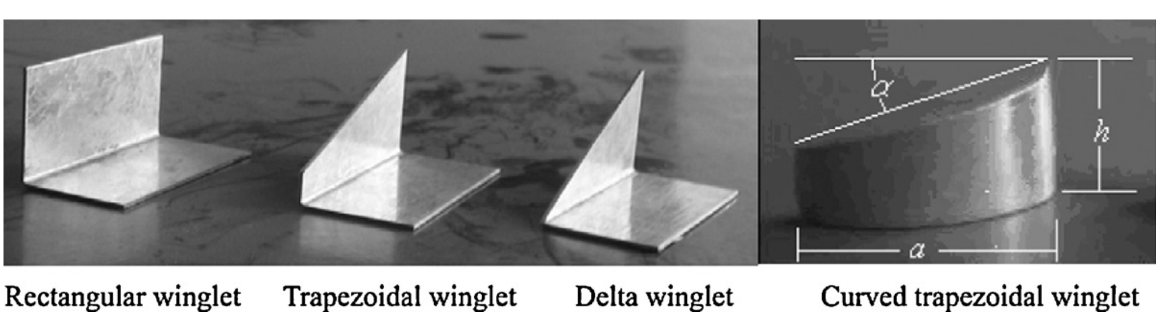


Fig. 38. Pictorial diagram of vortex generators.

8. Conclusion

Based on the review of the literature on turbulence promoters used in solar thermal systems, it has been found that small height roughness element of different configuration was widely investigated both analytically and experimentally and numerical studies also predict same the behavior as the experimental results. A number of studies have been carried out in order to investigate the effect of various parameters on the performance of asymmetrically heated rectangular duct. The relative roughness height, relative roughness pitch, angle of attack and relative gap position in discrete ribs are considered the important factors that affect the performance of solar air heater and heat exchanger. Delta winglets were used in solar thermal systems and found suitable to generate the vortexes which increase the heat transfer without much increase in friction factor. Maximum studies have been reported with small height roughness elements and suitable optimum parameters are available that help the designers for their effective efficiency performance in industrial applications viz. air heater, turbine blade cooling, nuclear reactor and electronic equipments. Few studies have been reported with high roughness height generally called baffles and they show high rate of heat transfer but baffle blockage increase the pressure drop which is a serious concern thus investigators must look to reduce the pressure drop which can attained by desecrating the geometry or to find the geometry which will be thermo-hydraulically better. Literature study on baffles reveals that the perforation is an effective technique in order to reduce the pressure drop without much reduction in heat transfer. Studies on transverse perforation baffle are reported by the investigators and they found that the perforated baffles are thermo-hydraulically better in comparison to solid baffles. No correlation is available in the literature which can predict their performance. The compound delta winglets can be used to enhance heat transfer and perforated winglets may found suitable in performance enhancement of solar thermal systems. Thus the there is tremendous scope for future study of the heat transfer and friction factor characteristics of different shapes of perforation baffle, delta winglets and the effect of hole sizing and its alignment. The information presented here will be beneficial for beginners in this area of research.

References

[1] Garg HP, Prakash J. Solar energy fundamentals and applications. New Delhi: Tata McGraw-Hill; 1997.
[2] Duffie JA, Beckman WA. Solar engineering of thermal processes. New York: Wiley; 1980.
[3] Frank K, Mark SB. Principles of heat transfer. Colorado: Thomson Learning Inc.; 2001.
[4] Bergles AE, Webb RL, Junkan GH. Energy conservation via heat transfer enhancement. Energy 1979;4:193–200.
[5] Mittal MK, Varun Saini RP, Singal SK. Effective efficiency of solar air heaters having different types of roughness elements on the absorber plate. Energy 2007;32:739–45.
[6] Webb RL, Eckert ERG. Heat transfer and friction in tubes with repeated-rib roughness. Int J Heat Mass Transfer 1971;14:601–17.
[7] Lewis MJ. Optimizing the thermohydraulic performance of rough surfaces. Int J Heat Mass Transfer 1975;18:1243–8.
[8] Ravigururajan TS, Bergles AE. General correlations for pressure drop and heat transfer for single-phase turbulent flow in internally ribbed tubes augmentation of heat transfer in energy systems. HTD, vol. 52. New York: ASME; 1985. p. 9–20.
[9] Han JC, Glicksman LR, Rohsenow WM. Heat transfer and friction for rib roughened surfaces. Int J Heat Mass Transfer 1978;21:1143–56.
[10] Han JC. Heat transfer and friction in channels with opposite rib roughened walls. Trans ASME J Heat Transfer 1984;106:774–81.
[11] Han JC, Park JS. Developing heat transfer in a rectangular channel with rib turbulators. ASME J Heat Transfer 1988;31:183–95.
[12] Han JC, Ou S, Park JS, Lei CK. Augmented heat transfer in rectangular channels of narrow aspect ratio with rib turbulators. Int J Heat Mass Transfer 1989;32:1619–30.
[13] Han JC, Zhang YM, Lee CP. Influence of surface heat flux ratio on heat transfer augmentation in square channel with parallel, crossed and V-shaped angled ribs. ASME J Turbomachinery 1994;114:872–80.
[14] Liou TM, Hwang JJ. Effect of ridge shapes on turbulent heat transfer and friction in a rectangular channel. Int J Heat Mass Transfer 1993;36:931–40.
[15] Lau SC, Kukreja RT, McMillin RD. Effects of V shaped rib arrays on turbulent heat transfer and friction of fully developed flow in a square channel. Int J Heat Mass Transfer 1991;34:1605–16.
[16] Taslim ME, Li T, Kercher DM. Experimental heat transfer and friction in channels roughened with angled, V-shaped and discrete ribs on two opposite walls. ASME J Turbomachinery 1996;118:20–8.
[17] Olsson CO, Sunden B. Thermal and hydraulic performance of a rectangular duct with multiple V-shaped ribs. Trans ASME 1998;120:1072–7.
[18] Gao X, Sunden B. Heat transfer and pressure drop measurements in rib roughened rectangular ducts. Exp Therm Fluid Sci 2001;24:25–34.
[19] Hu Z, Shen J. Heat transfer enhancement in a converging passage with discrete ribs. Int J Heat Mass Transfer 1996;39:1719–27.
[20] Cho HH, Wu SJ, Kwon HJ. Local heat/mass transfer measurement in a rectangular duct with discrete ribs. J Turbomachinery 2000;122:579–86.
[21] Chyu MK, Yu Y, Ding H, Downs JP, Seochting F. Concavity enhanced heat transfer in an internal cooling passage. In: ASME 42nd international gas turbine and aero congress; 1997 [paper no. 97-GT-437].
[22] Chyu MK, Yu Y, Ding H, Downs JP, Seochting F. Heat transfer enhancement in rectangular channels with concavities. Enhanced Heat Transfer 1999;6:429–39.
[23] Moon HK, O'Connell T, Glezer B. Channel height effect on heat transfer and friction in a dimpled passage. ASME J Eng Gas Turbines Power 2000;122:307–13.
[24] Mahmood GI, Hill ML, Nelson DL, Ligrani PM, Moon HK, Glezer B. Local heat transfer and flow structure on and above a dimpled surface in a channel. ASME Trans Turbomachinery 2001;123:115.
[25] Mahmood GI, Ligrani PM. Heat transfer in a dimpled channel: combined influences of aspect ratio, temperature ratio, Reynolds number and flow structure. Int J Heat Mass Transfer 2002;45:2011–20.
[26] Burgess NK, Oliveira MM, Ligrani PM. Nusselt number behaviour on deep dimpled surfaces within a channel. J Heat Transfer 2003;125:11–8.
[27] Sang DH, Hyun GK, Hyung HC. Heat transfer with dimple/protrusion arrays in a rectangular duct with low Reynolds number range. Int J Heat Fluid Flow 2008;29:916–26.
[28] Chang SW, Chiang KF, Yang TL, Huang CC. Heat transfer and pressure drop in dimpled fin channels. Exp Therm Fluid Sci 2008;33:23–40.
[29] Varun, Saini RP, Singal SK. A review on roughness geometry used in solar air heaters. Sol Energy 2007;81:1340–50.
[30] Hong YJ, Hsieh SS. An experimental investigation of heat transfer characteristics for turbulent flow over staggered ribs in a square duct. Exp Therm Fluid Sci 1991;4:714–22.
[31] Park JS, Han JC, Huang Y, Ou S. Heat transfer performance comparisons of five different rectangular channels with parallel angled ribs. Int J Heat Mass Transfer 1992;35:2891–903.
[32] Olsson CO, Sunden B. Experimental study of flow and heat transfer in rib-roughened rectangular channels. Exp Therm Fluid Sci 1998;16:349–65.
[33] Murata A, Mochizuki S. Comparison between laminar and turbulent heat transfer in a stationary square duct with transverse or angled rib turbulators. Int J Heat Mass Transfer 2000;44:1127–41.
[34] Tariq A, Singh K, Panigrahi PK. Detailed measurement of heat transfer and flow characteristics in rectangular duct with rib turbulators mounted on the bottom surface. Eng Turb Model Exp 2002;5:445–54.
[35] Tatsumi K, Iwai H, Inaoka K. Numerical simulation for heat and fluid characteristics of square duct with discrete rib turbulators. Int J Heat Mass Transfer 2002;45:4353–9.
[36] Cavallero D, Tanda G. An experimental investigation of forced convection heat transfer in channels with rib turbulators by means of liquid crystal thermography. Exp Therm Fluid Sci 2002;26:115–21.
[37] Wong TT, Leung CW, Li ZY, Tao WQ. Turbulent convection of air cooled rectangular duct with surface mounted cross ribs. Int J Heat Mass Transfer 2003;46:4629–38.
[38] Tanda G. Heat transfer in rectangular channels with transverse and V shaped broken ribs. Int J Heat Mass Transfer 2004;47:229–43.
[39] Won SY, Ligrani. Comparisons of flow structure and local Nusselt numbers in a channels with parallel and crossed rib turbulators. Int J Heat Mass Transfer 2004;47:1573–86.
[40] Lu B, Jiang PX. Experimental and numerical investigation of convection heat transfer in a rectangular channel with angled ribs. Exp Therm Fluid Sci 2006;30:513–21.
[41] Kamali R, Binesh AR. The importance of rib shape effects on the local heat transfer and flow friction characteristics of square ducts with ribbed internal surfaces. Int Commun Heat Mass Transfer 2008;35:1032–40.
[42] Promvonge P, Thianpong C. Thermal performance assessment of turbulent channel flows over different shaped ribs. Int Commun Heat Mass Transfer 2008;35:1327–34.
[43] Thianpong C, Chompookham T, Skullong S, Promvonge P. Thermal characterization of turbulent flow in a channel with isosceles triangular ribs. Int Commun Heat Mass Transfer 2009;36:712–7.
[44] Lee DH, Rhee DH, Kim KM, Cho HH, Moon HK. Detailed measurement of heat/mass transfer with continuous and multiple V shaped ribs in rectangular channel. Energy 2009;37:1770–8.

[45] Tanda G. Effect of rib spacing on heat transfer and friction in a rectangular channel with 45° angled rib turbulators on one/two walls. Int J Heat Mass Transfer 2011;54:1081–90.
[46] Kays WB. Convective heat and mass transfer. New York: McGraw Hill Book Co.; 1966. p. 197–8.
[47] Prasad BN, Saini JS. Effect of artificial roughness on heat transfer and friction factor in a solar air heater. Sol Energy 1988;41:555–60.
[48] Prasad BN, Saini JS. Optimal thermo hydraulic performance of artificially roughened solar air heaters. Sol Energy 1991;47:91–6.
[49] Gupta D, Solanki SC, Saini JS. Heat and fluid flow in rectangular solar air heater ducts having transverse rib roughness on absorber plates. Sol Energy 1993;51:31–7.
[50] Verma SK, Prasad BN. Investigation for the optimal thermo hydraulic performance of artificially roughened solar air heaters. Renew Energy 2000;20:19–36.
[51] Sahu MM, Bhagoria JL. Augmentation of heat transfer coefficient by using 90° broken transverse ribs on absorber plate of solar air heater. Renew Energy 2005;30:2057–63.
[52] Gupta D, Solanki SC, Saini JS. Thermo hydraulic performance of solar air heaters with roughened absorber plates. Sol Energy 1997;61:33–42.
[53] Muluwork KB, Saini JS, Solanki SC. Studies on discrete rib roughened solar air heaters. In: Proceedings of national solar energy convention. 1998. p. 75–84.
[54] Muluwork KB. Investigations on fluid flow and heat transfer in roughened absorber solar heaters. Ph.D. Thesis, IIT, Roorkee; 2000.
[55] Momin AME, Saini JS, Solanki SC. Heat transfer and friction in solar air heater duct with V-shaped rib roughness on absorber plate. Int J Heat Mass Transfer 2002;45:3383–96.
[56] Karwa R. Experimental studies of augmented heat transfer and friction in asymmetrically heated rectangular ducts with ribs on the heated wall in transverse, inclined, v-continuous and v-discrete pattern. Int Commun Heat Mass Transfer 2003;30:241–50.
[57] Karmare SV, Tikekar AN. Heat transfer and friction factor correlation for artificially roughened duct with metal grit ribs. Int J Heat Mass Transfer 2007;50:4342–51.
[58] Aharwal KR, Gandhi BK, Saini JS. Experimental investigation on heat-transfer enhancement due to a gap in an inclined continuous rib arrangement in a rectangular duct of solar air heater. Renew Energy 2008;33:585–96.
[59] Varun Saini RP, Singal SK. Investigation of thermal performance of solar air heater having roughness elements as a combination of inclined and transverse ribs on the absorber plate. Renew Energy 2008;33:1398–405.
[60] Saini SK, Saini RP. Development of correlations for Nusselt number and friction factor for solar air heater with roughened duct having arc-shaped wire as artificial roughness. Sol Energy 2008;82:1118–30.
[61] Hans VS, Saini RP, Saini JS. Heat transfer and friction factor correlations for a solar air heater duct roughened artificially with multiple v ribs. Sol Energy 2010;84:898–991.
[62] Singh S, Chander S, Saini JS. Heat transfer and friction factor correlations of solar air heater ducts artificially roughened with discrete v-down ribs. Energy 2011;36:5053–64.
[63] Karwa R, Solanki SC, Saini JS. Heat transfer coefficient and friction factor correlations for the transitional flow regime in rib-roughened rectangular ducts. Int J Heat Mass Transfer 1999;42:1597–615.
[64] Bhagoria JL, Saini JS, Solanki SC. Heat transfer coefficient and friction factor correlations for rectangular solar air heater duct having transverse wedge shaped rib roughness on the absorber plate. Renew Energy 2002;25:341–69.
[65] Jaurker AR, Saini JS, Gandhi BK. Heat transfer and friction characteristics of rectangular solar air heater duct using rib-grooved artificial roughness. Sol Energy 2006;80(8):895–907.
[66] Layek A, Saini JS, Solanki SC. Second law optimization of a solar air heater having chamfered rib-groove roughness on absorber plate. Renew Energy 2007;32:1967–80.
[67] Saini RP, Saini JS. Heat transfer and friction factor correlations for artificially roughened ducts with expended metal mesh as roughness element. Int J Heat Mass Transfer 1997;40(4):973–86.
[68] Saini RP, Verma J. Heat transfer and friction factor correlations for a duct having dimple-shape artificial roughness for solar air heaters. Energy 2008;33:1277–87.
[69] Bhushan B, Singh R. Nusselt number and friction factor correlations for solar air heater duct having artificially roughened absorber plate. Sol Energy 2011;85:1109–18.
[70] Yeh HM, Chou WH. Efficiency of solar air heaters with baffles. Energy 1991;16:983–7.
[71] Yeh HM, Ho CD, Lin CY. The influence of collector aspect ratio on the collector efficiency of baffled solar air heaters. Energy 1998;23:11–6.
[72] Mousavi SS, Hooman K. Heat and fluid flow in entrance region of a channel with staggered baffles. Energy Convers Manage 2006;47:2011–9.
[73] Romdhane BS. The air solar collectors: comparative study, introduction of baffles to favor the heat transfer. Sol Energy 2007;81:139–49.
[74] Sripattanapipat S, Promvonge P. Numerical analysis of laminar heat transfer in a channel with diamond shaped baffles. Int Commun Heat Mass Transfer 2009;36:32–8.
[75] Nie JH, Chen YT, Hsieh HT. Effects of a baffle on separated convection flow adjacent to backward facing step. Int J Therm Sci 2009;48:618–25.
[76] Bopche SB, Tandale MS. Experimental investigation on heat transfer and frictional characteristics of a turbulator roughened solar air heater duct. Int J Heat Mass Transfer 2009;52:2834–48.
[77] Promvonge P. Heat transfer and pressure drop in a channel with multiple 60° V baffles. Int Commun Heat Mass Transfer 2010;37:835–40.
[78] Promvonge P, Jedsadaratanachai W, Kwankaomeng S. Numerical study of laminar flow and heat transfer in square channel with 30° inline angled baffle turbulators. Appl Therm Eng 2010;30:1292–303.
[79] Kwankaomeng S, Promvonge P. Numerical prediction on laminar heat transfer in square duct with 30° angled baffle on one wall. Int Commun Heat Mass Transfer 2010;37:857–66.
[80] Promvonge P, Kwankaomeng S. Periodic laminar flow and heat transfer in a channel with 45° staggered V baffles. Int Commun Heat Mass Transfer 2010;37:841–9.
[81] Yang YT, Hwang CZ. Calculation of turbulent flow and heat transfer in a porous baffled channel. Int J Heat Mass Transfer 2003;46:771–80.
[82] Ko KH, Anand NK. Use of porous baffles to enhance heat transfer in a rectangular channel. Int J Heat Mass Transfer 2003;46:4191–9.
[83] Tzeng SC, Jeng TM, Wang YC. Experimental study of forced convection in asymmetrically heated sintered porous channels with/without periodic baffles. Int J Heat Mass Transfer 2006;49:78–88.
[84] Molki M, Mostoufizadeh. Turbulent heat transfer in rectangular ducts with repeated baffle blockages. Int J Heat Mass Transfer 1989;32:1491–9.
[85] Hwang JJ, Liou TM. Heat transfer in a rectangular channel with perforated turbulence promoters using holographic interferometry measurement. Int J Heat Mass Transfer 1995;38:3197–207.
[86] Hwang JJ, Lia TY, Liou TM. Effect of fence thickness on pressure drop and heat transfer in a perforated fenced channel. Int J Heat Mass Transfer 1998;41:811–6.
[87] Liou TM, Chen SH. Turbulent heat and fluid flow in a passage distributed by detached perforated ribs of different heights. Int J Heat Mass Transfer 1998;41:1795–806.
[88] Li H, Kottke V. Effect of baffle spacing on pressure drop and local heat transfer in shell and tube heat exchangers for staggered tube arrangement. Int J Heat Mass Transfer 1998;41:1303–11.
[89] Dutta, Dutta. Effect of baffle size, perforation, and orientation on internal heat transfer enhancement. Int J Heat Mass Transfer 1998;41:3005–13.
[90] Dutta P, Hossain A. Internal cooling augmentation in rectangular channel using two inclined baffles. Int J Heat Fluid Flow 2005;26:223–32.
[91] Karwa R, Maheshwari BK, Karwa N. Int Commun Heat Mass Transfer 2005;32:275–84.
[92] Lin CW. Experimental study of thermal behaviors in a rectangular channel with baffle of pores. Int Commun Heat Mass Transfer 2006;33:985–92.
[93] Huang KD, Tzeng SC, Jeng TM, Wang JR, Cheng SY, Tseng KT. Experimental study of fluid flow and heat transfer characteristics in the square channel with a perforation baffle. Int Commun Heat Mass Transfer 2008;35:1106–12.
[94] Karwa R, Maheshwari BK. Heat transfer and friction in an asymmetrically heated rectangular duct with half and fully perforated baffles at different pitches. Int Commun Heat Mass Transfer 2009;36:264–8.
[95] Hans VS, Saini RP, Saini JS. Performance of artificially roughened solar air heaters—a review. Renew Sustain Energy Rev 2009;13:1854–69.
[96] Gentry MC, Jacobi AM. Heat transfer enhancement by delta-wing vortex generators on a flat plate: vortex interactions with the boundary layer. Exp Therm Fluid Sci 1997;14:231–42.
[97] Torii K, Kwak KM, Nishino K. Heat transfer enhancement accompanying pressure loss reduction with winglet type vortex generators for fin tube heat exchangers. Int J Heat Mass Transfer 2002;45:3795–801.
[98] Yakut K, Sahin B, Celik C, Alemdaroglu N, Kurnuc A. Effect of tapes with double sided delta winglets on heat and vortex characteristics. Appl Energy 2005;80:77–95.
[99] Joardar A, Jacobi AM. Heat transfer enhancement by winglet type vortex generator arrays in compact plain fin and tube heat exchanger. Int J Refrig 2008;31:87–97.
[100] Tian L, He Y, Tao Y, Tao W. A comparative study on the air side performance of wavy fin and tube heat exchanger with punched delta winglets in staggered and inline arrangements. Int J Therm Sci 2009;48:1765–76.
[101] Min C, Qi C, Kong X, Dong J. Experimental study of rectangular channel with modified rectangular longitudinal vortex generators. Int J Heat Mass Transfer 2010;53:3023–9.
[102] Kotcioglu I, Caliskan S, Cansiz A, Baskaya S. Second law analysis and heat transfer in a cross flow heat exchanger with a new winglet type vortex generator. Energy 2010;35:3686–95.
[103] Eiamsa-ard S, Wongcharee K, Eiamsa-ard P, Thianpong C. Heat transfer enhancement in a tube using delta winglet twisted tapes inserts. Appl Therm Eng 2010;30:310–8.
[104] Chompookham T, Thianpong C, Kwankaomeng S, Promvonge P. Heat transfer augmentation in a wedge ribbed channel using winglet vortex generators. Int Commun Heat Mass Transfer 2010;37:163–9.
[105] Promvonge P, Khanoknaiyakarn C, Kwankaomeng S, Thianpong C. Thermal behavior in solar air heater channel fitted with combined rib and delta-winglet. Int Commun Heat Mass Transfer 2011;38:749–56.
[106] Zhou G, Ye Q. Experimental investigations of thermal and flow characteristics of curved trapezoidal winglet type vortex generators. Appl Therm Eng 2012;37:241–8.
[107] Bhushan B, Singh R. A review on methodology of artificial roughness used in duct of solar air heaters. Energy 2010;35:202–12.
[108] Gupta D. Investigations on fluid flow and heat transfer in solar air heaters with roughened absorbers. PhD.Thesis. India: University of Roorkee; 1994.